

The low-redshift Ly α forest towards 3C 273[★]

Gerard M. Williger,^{1,2,3,4†} Robert F. Carswell,⁵ Ray J. Weymann,⁶ Edward B. Jenkins,⁷
Kenneth R. Sembach,⁸ Todd M. Tripp,⁹ Romeel Davé,¹⁰ Lutz Habertzettl³
and Sara R. Heap¹

¹Code 667, NASA Goddard Space Flight Center, Greenbelt, MD 20771, USA

²Department of Physics & Astronomy, Johns Hopkins University, Baltimore, MD 21218, USA

³Department of Physics & Astronomy, University Louisville, Louisville, KY 40292, USA

⁴Present address: Lab. Fizeau, Univ. de Nice, UMR 6525, 06108 Nice Cedex 2, France

⁵Institute of Astronomy, Madingley Road, Cambridge CB3 0HA

⁶Carnegie Observatories, 813 Santa Barbara St, Pasadena, CA 91101, USA

⁷Princeton University Observatory, Princeton, NJ 08544, USA

⁸Space Telescope Science Institute, Baltimore, MD 21218, USA

⁹Department of Astronomy, University of Massachusetts, Amherst, MA 01003, USA

¹⁰Department of Astronomy, University of Arizona, Tucson, AZ 85721, USA

Accepted 2010 February 18. Received 2010 February 18; in original form 2009 November 8

ABSTRACT

We present an analysis of the Ly α forest towards 3C 273 from the Space Telescope Imaging Spectrograph at ~ 7 km s⁻¹ resolution, along with reprocessed data from the *Far Ultraviolet Spectroscopic Explorer*. The high ultraviolet flux of 3C 273 allows us to probe the weak, low- z absorbers. The main sample consists of 21 H I absorbers that we could discriminate to a sensitivity of $\log N_{\text{H I}} \approx 12.5$. The redshift density for absorbers with $13.1 < \log N_{\text{H I}} < 14.0$ is $\sim 1.5\sigma$ below the mean for other lines of sight; for $\log N_{\text{H I}} \geq 12.5$, it is consistent with numerical model predictions. The Doppler parameter distribution is consistent with other low- z samples. We find no evidence for a break in the column density power-law distribution to $\log N_{\text{H I}} = 12.3$. A broad Ly α absorber is within $\Delta v \leq 50$ km s⁻¹ and 1.3 local-frame Mpc of two $\sim 0.5L^*$ galaxies, with an O VI absorber ~ 700 km s⁻¹ away, similarly close to three galaxies and indicating overdense environments. We detect clustering on the $\Delta v < 1000$ km s⁻¹ scale at 3.4σ significance for $\log N_{\text{H I}} \geq 12.6$, consistent with the level predicted from hydrodynamical simulations, and indication for a Ly α forest void at $0.09 < z < 0.12$. We find at least two components for the $z = 0.0053$ Virgo absorber, but the total $N_{\text{H I}}$ column is not significantly changed.

Key words: intergalactic medium – quasars: absorption lines – cosmology: observations.

1 INTRODUCTION

The low-redshift Ly α forest offers both a challenge and an opportunity to study the physics of the intergalactic medium (IGM) and its role in galaxy formation and evolution. The challenge is the requirement for space-based UV spectroscopy, which is undergoing a

renewal with the installation of Cosmic Origins Spectrograph (COS) on *HST*. The opportunity is to observe absorption systems at small enough distances to be able to relate nearby galaxy characteristics far down the luminosity function. The calculation and interpretation of numerical models using the fluctuating Gunn–Peterson approximation (e.g. Croft et al. 1998) greatly benefit from constraints on the end epoch for absorber distribution functions such as number densities, column densities, Doppler parameters, clustering and relations to galaxies. A consequence of the models is that the low- z Ly α forest is predicted to harbour a significant fraction of the baryons, as is a hot shocked component (e.g. Cen & Ostriker 1999; Davé et al. 1999; Davé et al. 2001). For a given column density, the low- z forest is predicted to probe larger mass overdensities than at high redshift, which adds complexity to comparisons of absorber property distribution functions between widely differing epochs.

[★]Based on observations with (1) the NASA/ESA *Hubble Space Telescope*, obtained at the Space Telescope Science Institute, which is operated by the Association of Universities for Research in Astronomy, Inc., under NASA contract NAS 05-26555, and (2) the NASA-CNES/ESA *Far Ultraviolet Spectroscopic Explorer* mission, operated by the Johns Hopkins University, supported by NASA contract NAS 05-32985.

†E-mail: williger@physics.louisville.edu

Exploration of the $z < 1.6$ Ly α forest began in earnest with *HST* observations of the brightest quasi-stellar object (QSO), 3C 273, using the Faint Object Spectrograph (Bahcall et al. 1991) and Goddard High Resolution Spectrograph (Morris et al. 1991), which revealed five and 10 Ly α absorbers, respectively. The main result was that there were many more low-redshift systems than expected from a simple extrapolation from $z > 2$ of the decline of the absorber redshift density over time. Concurrently, observations of the galaxy environments around Ly α absorbers were made, again with the 3C 273 field among the first to be probed, which revealed a complex relationship between absorbers and galaxies. The absorber–galaxy correlation was found to be stronger than random, but not as strong as the galaxy–galaxy correlation (Salzer 1992; Morris et al. 1993; Lanzetta et al. 1995; Stocke et al. 1995; Shull, Stocke & Penton 1996; Tripp, Lu & Savage 1998), a trend which has held up in recent years (e.g. Chen et al. 2005; Prochaska et al. 2006). Using H I-selected galaxies, however, Ryan-Weber (2006) found the absorber–galaxy correlation even stronger than the galaxy autocorrelation on ~ 1 –15 Mpc scales.

Over the last 17 yr, great efforts were made to accumulate observations of a number of low-redshift QSOs. A leap in observing efficiency came with the installation of Space Telescope Imaging Spectrograph (STIS) in 1997. Crucial access to higher order Lyman lines was provided by the launch of the *Far Ultraviolet Spectroscopic Explorer* (*FUSE*) in 1999. To date, a few hundred low- z Ly α forest lines have been observed at resolutions down to ~ 7 km s $^{-1}$. Such works typically involved studies of one to a few sightlines at a time e.g. Williger et al. (2006, hereafter Paper I), but more recently therein large analyses of archival data, including recent works by Lehner et al. (2007a), Danforth & Shull (2008), and Wakker & Savage (2009). The H I column density distribution shows evidence of a slight steepening at low z compared to that at $z \gtrsim 2$ (e.g. Lehner et al. 2007a, and references therein), and also a small increase in the mean Doppler parameter (b) over time. An excess of broad Ly α absorbers (BLAs) with $b > 40$ km s $^{-1}$ at $z \lesssim 0.5$ is also observed, which is attributed to a larger fraction of warm-hot IGM (WHIM) gas at low z , consistent with model predictions; this population of BLAs is currently the subject of active study (e.g. Richter, Fang & Bryan 2006a; Richter et al. 2006b; Tripp et al. 2008; Wakker & Savage 2009). Recent observational estimates for the baryon contribution of the low- z Ly α forest are 30 per cent or more (Penton, Shull & Stocke 2004; Lehner et al. 2007a). Danforth & Shull (2008) argue that low- z O VI absorbers reveal 10 per cent of the baryons in warm-hot gas, but Tripp et al. (2008) have shown that many of the O VI lines are well aligned with narrow H I lines, and in those cases, the O VI absorber properties suggest an origin in cool, photoionized gas. (A similar conclusion is favoured by Thom & Chen 2008.) Indeed, Oppenheimer & Davé (2009) have argued that most low- z O VI systems are photoionized based on their hydrodynamic simulations of large-scale structures. However, some O VI absorbers show strong evidence of hot gas (e.g. Tripp et al. 2001; Savage et al. 2005; Narayanan, Wakker & Savage 2009). Larger statistical studies employing more robust diagnostics are required to reliably interpret the natures of O VI absorbers.

3C 273 has always been one of the first extragalactic targets observed with new technology for a variety of astronomical topics (e.g. Ulrich et al. 1980). In addition to 3C 273 being extremely bright, it also lies behind the Virgo cluster, which makes it particularly useful for studies of absorber–galaxy relations and the physical conditions in halo and filament gas, from the cluster out to the vicinity of the QSO. In a partial listing of successor projects after the early *HST* papers cited above, the sightline was the subject of fur-

ther Goddard High Resolution Spectrograph (GHRS) observations (Weymann et al. 1995) and a number of galaxy studies relating to absorber environments (e.g. Salpeter & Hoffman 1995; Hoffman et al. 1998; Grogin, Geller & Huchra 1998; Impey, Petry & Flint 1999). Sembach et al. (2001) explored the Ly β forest of 3C 273 with *FUSE*, and Tripp et al. (2002) examined the physical states of two high column density Virgo cluster absorbers. Rosenberg et al. (2003) compared Virgo metal systems towards RXJ1230.8+0115, which is the nearest bright low-redshift QSO ($z = 0.117$, 55 arcmin away), and concluded that a large-scale structure filament may produce correlated absorption.

Preliminary results for ~ 7 km s $^{-1}$ resolution STIS echelle spectroscopy of 3C 273 were presented by Heap et al. (2002) and Heap et al. (2003). We present a full analysis here, including a coverage of Galactic and IGM absorption system parameters. We also make use of complementary data from *FUSE*, with recent improvements in data processing, reduction and analysis. The QSO 3C 273 lies at Galactic $l = 289.95$, $b = 64.36$, and thus serves as a very useful probe of the Galactic halo. Over wavelengths covered by the Ly α forest, our data have S/N = 20–30 per ~ 3.2 km s $^{-1}$ pixel with 1.7 pixels per resolution element at 1200 Å (Dressel et al. 2007), except for small dips at the ends of orders. The superior signal and resolution of our data permit us to probe the low- z Ly α forest to $\log N_{\text{H I}} \sim 12.3$ –12.5, which is the best observation done to date, regardless of resolution. This column density limit corresponds to mass overdensities of $\log(\rho_{\text{H}}/\bar{\rho}_{\text{H}}) \sim 0.4 \pm 0.2$ (Davé et al. 1999; Davé & Tripp 2001) as calculated from hydrodynamical models in the cold dark matter (CDM) scenario. Similar mass overdensities at $z \sim 3$ correspond to $\log N_{\text{H I}} \sim 14.0$ –14.5 (though the true density–column density relation is likely complex due to the non-linear growth of large perturbations). The high S/N of our spectrum also allows us to detect BLAs with good efficiency. The study of hot halo gas for the Virgo absorbers along this sightline (Tripp et al. 2002, 2008) prompted us to verify the component structure of the $z = 0.0053$ absorber with the *FUSE* data. While a number of recent Ly α forest publications tend to include more and more sightlines per paper, our focus on the single sightline of 3C 273 merits an in-depth analysis of the Ly α forest from a special perspective, due to the high quality of the spectrum and the value added by existing and future deep galaxy surveys in the region.

This paper is organized as follows. We describe the STIS and *FUSE* observations in Section 2. The absorption line selection procedure details are in Section 3, as are a list of Galactic absorption lines in the STIS data and an upper limit on C IV absorption for a high H I column density absorber at $z = 0.0665$. We explain our simulations to constrain the probability of feature detection in Section 3.4. Our results and discussion for the Ly α forest, BLAs and their relation to O VI absorbers and galaxies, clustering and voids, and the $z = 0.0053$ Virgo absorber velocity structure are in Section 4. Our conclusions are summarized in Section 5. We adopt a cosmology of $H_0 = 70$ km s $^{-1}$ Mpc $^{-1}$, $\Omega_b = 0.3$ and $\Lambda = 0.7$ throughout this paper.

2 OBSERVATIONS AND REDUCTIONS

2.1 STIS spectra

3C 273 was observed with *HST* and STIS using guaranteed time from Program 8017 to the STIS Instrument Definition Team (IDT). The instrumental set-up used grating E140M for seven orbits (18671 sec) on 2000 May 2 and 2000 June 21–22, with the 0.2×0.2 arcsec 2 slit. For the E140M grating, the STIS Instrument

Handbook gives a dispersion of $\lambda/91700 \text{ \AA pixel}^{-1}$, a full width at half-maximum for the line spread function for the $0.2 \times 0.2 \text{ arcsec}^2$ slit of 1.4 and 1.3 pixels at 1200 and 1500 \AA , respectively, and a resolving power for a two-pixel resolution element of 45 800.

The data were processed and spectra extracted with CALSTIS and a suite of programs from the STIS ID Team at Goddard Space Flight Centre, including corrections for scattered light and hot pixels and customized merging of echelle orders to minimize echelle ripple (written by Don Lindler). We constructed a continuum using a combination of routines from automated AUTOVP (Davé, Dubinski & Hernquist 1997) and interactive LINE_NORM routines (D. Lindler) because the regions around emission lines were best done with manual fitting. Longward of our Ly α forest sample region, two regions at 1402–1405 and 1425–1430 \AA were lost due to vignetting from the STIS repeller wire. The total STIS wavelength coverage is 1142–1709 \AA . Redward of 1616 \AA , there are five small (0.15–0.58 \AA) interorder gaps.

2.2 FUSE spectra

We use FUSE spectra from the principal investigator program P10135. An analysis of the FUSE data was done by Sembach et al. (2001), which employed a customized version of the FUSE pipeline CALFUSE 1.8.7. In this study, we used similar techniques and CALFUSE 3.1.3. We screened the data for valid photon events, registered the individual spectra by cross-correlating on the interstellar features, and set the zero-point by cross referencing with HST data for interstellar lines. Both the FUSE LiF and SiC channel data show some improvement in terms of resolution. In the 2001 reduction, the screening limits for pulse height distribution were (manually) set with care, but in this work, the wider default values were used. The use of these wider values was able to reduce the noise compared to the earlier reduction. Aside from a small stretch in the LiF2 data and cases where a feature fell on a fibre bundle boundary, the velocity scale is generally good to $\pm 5 \text{ km s}^{-1}$, save for a few cases where there is an offset of as much as half a resolution element (22–25 km s^{-1}). The SiC backgrounds are good except for SiC1 at $\lambda < 920 \text{ \AA}$. We refer the reader to Sembach et al. for further details.

For profile fitting, we originally used night-only FUSE data; later we tried using all of the data but found no significant improvement in the results. Continua for the FUSE spectra were created using interactive LINE_NORM routines. We permitted velocity offsets as a free parameter on the order of the FUSE uncertainties as needed to improve individual fits. Absorption system parameters presented in this paper use the night-only data.

3 ABSORPTION LINES

3.1 Selection

Absorption line selection was a multistep process. We began the process by pre-selecting an inclusive line list using a series of selection criteria based on significance. Our initial step was to make a preliminary selection of absorption features from the summed STIS data down to the 4.0σ significance level with a Gaussian filter based on the AUTOVP routine, with half-widths of 8, 12, 16 and 20 pixels. The large width provides sensitivity to BLAs and partially resolved complexes. As a further preliminary (and complementary) constraint, we then only included significant features within the regions flagged as significant in absorption with a simple equivalent width significance criterion, based on a $\sim 3.3\sigma$ threshold

for contiguous pixels below the continuum; such a criterion is more sensitive to narrow absorbers. Whenever possible, we confirmed spectral features by using the FUSE data. In particular, all (nine out of nine) absorbers with $\log N_{\text{H I}} \geq 13.24$ over $0.003 < z < 0.147$ were confirmed by inspection of Ly β data, and Ly β inspections showed no useful information for lower column density Ly α forest systems. The selection algorithm to this point was designed to be largely objective and repeatable, aside from continuum fitting around emission features. We then visually checked each absorption feature to avoid including noise spikes or potential continuum errors.

We subsequently tested the effectiveness of this selection technique by subjecting it to simulated spectra with similar resolution to the data to determine the 80 per cent detection probability based on a grid of Doppler parameters, H I column densities and S/N values. Details are in Section 3.3. The decrease in detection probability drops steeply from nearly 100 per cent to nearly zero over 0.1 dex in column density for a given S/N and Doppler parameter, which enables straightforward determinations of the 80 per cent detection efficiency to $\lesssim 0.05$ dex accuracy. Such a steep decline is not unreasonable given that the absorbers are of such low column density ($\log N_{\text{H I}} \sim 12.5$) that they are well on the linear part of the curve of growth. Their equivalent widths change little over the limited range of Doppler parameters and S/N (factors of 2) which we explored, and their velocity widths also only vary over a small interval. Therefore, when detecting weak but significant features relying in part on a boxcar approximation to an absorption profile, a range of 0.3 dex (a factor of 2) in column density would be a large range to expect a uniform detection threshold probability.

We made a concentrated effort to understand the rate of false detections, due to our desire to probe as deeply as possible down the H I column density distribution. Therefore, as an additional test, we examined the spectrum $> 5000 \text{ km s}^{-1}$ redward of the QSO's Ly α emission all the way to the red end of the STIS data (1710 \AA) for unidentified absorption features to test for the frequency of appearance of potential spurious features. The most significant one at 1667.9 \AA had a significance 2.3σ , which was well below our preliminary selection threshold. It would have Ly α fitting parameters of $\log N_{\text{H I}} = 12.53 \pm 0.13$ and Doppler parameter $b = 13.4 \pm 6.3$. The relatively large (47 per cent) error in b would make it unlikely to be considered a reliable Ly α absorber, even if it had somehow been included in our preliminary absorber list. The feature does not correspond to any plausible metal line for any Ly α absorber in our sample. The final STIS E140M spectrum of 3C 273, with absorption systems marked, is shown in Fig. 1.

3.2 Profile fitting technique

The data were profile fitted with vPFIT¹ (Webb 1987) using Voigt profiles convolved with the local STIS line spread function taken from the STIS Instrument Handbook. Oscillator strengths are from the vPFIT atomic data list (2004 December version), based on Morton (2003). Multiple transitions were used for simultaneous fits whenever they could improve constraints on column densities and Doppler parameters. We also used, as necessary, the vPFIT capabilities to allow for offsets in the local continuum level and in velocity for each spectral interval used in a fit. The latter would in particular compensate for small velocity uncertainties in the FUSE data.

¹ <http://www.ast.cam.ac.uk/~rfc/vpfit.html>

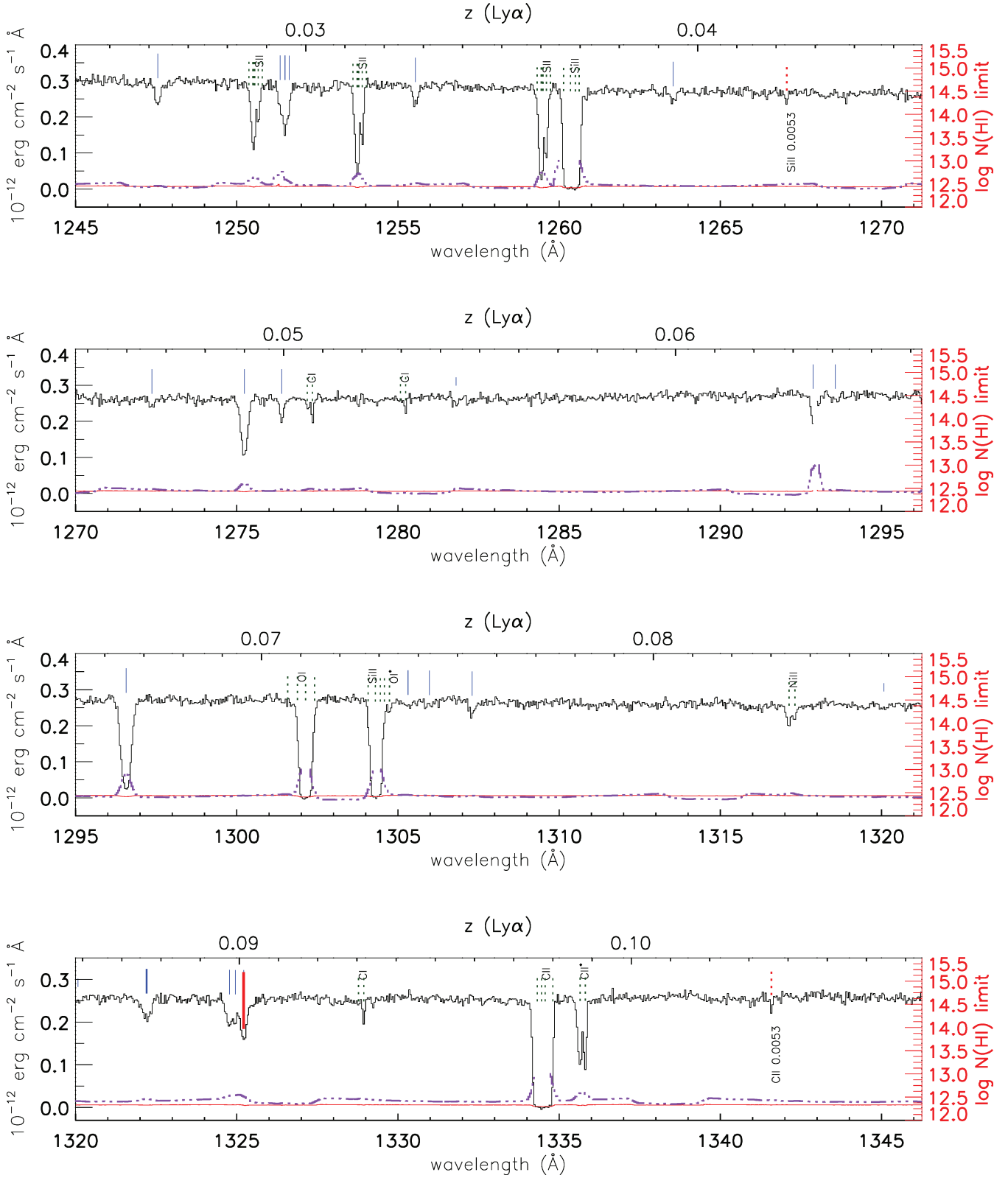


Figure 1 – continued

Doppler parameters were set to ranges with averages of 17.5, 22.2 or 24.7 and 35.0 km s^{-1} , and the input $\log N_{\text{HI}}$ values varied over 12.21–12.80 for $S/N = 20$ and 11.85–12.55 for $S/N = 40$. The simulated spectra were continuum-normalized, so any errors, sys-

tematic or random, involving continuum fitting are not reflected in the subsequent simulation analysis. There were also no noise spikes inserted into the spectra. We calculated statistics comparing the line parameters for simulated lines which were successfully

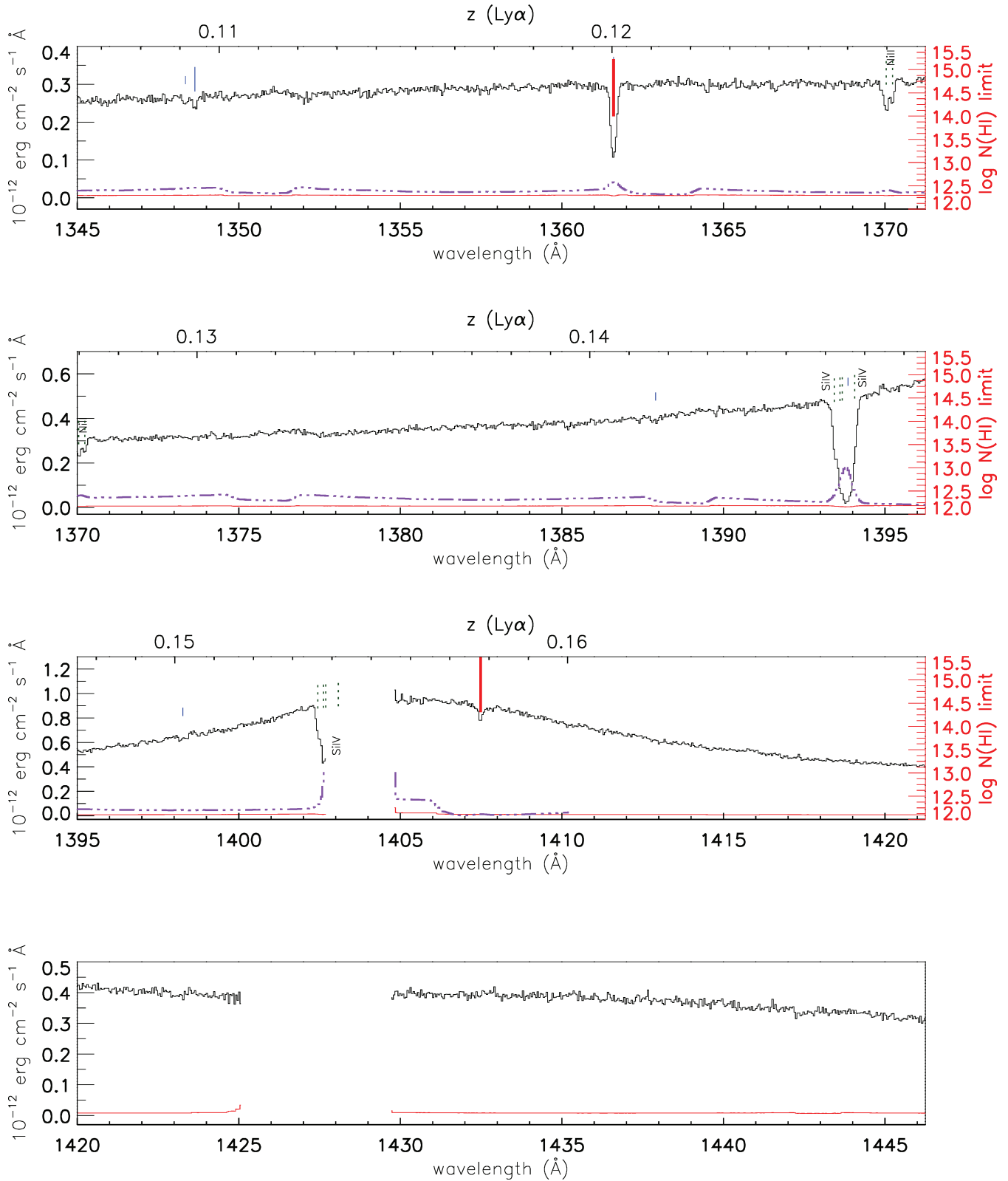


Figure 1 – continued

recovered versus the input values. Results for the various combinations of input S/N ratio and Doppler parameter are shown in Tables 1 and 2. The mean recovered measured Doppler parameters and column densities match the mean input values within the

mean of the profile fitting errors. The marginal tendency for the narrowest lines to be recovered with higher Doppler parameters is likely due to the effects of noise broadening input for features near the detection limit for recovered lines; noise which would make

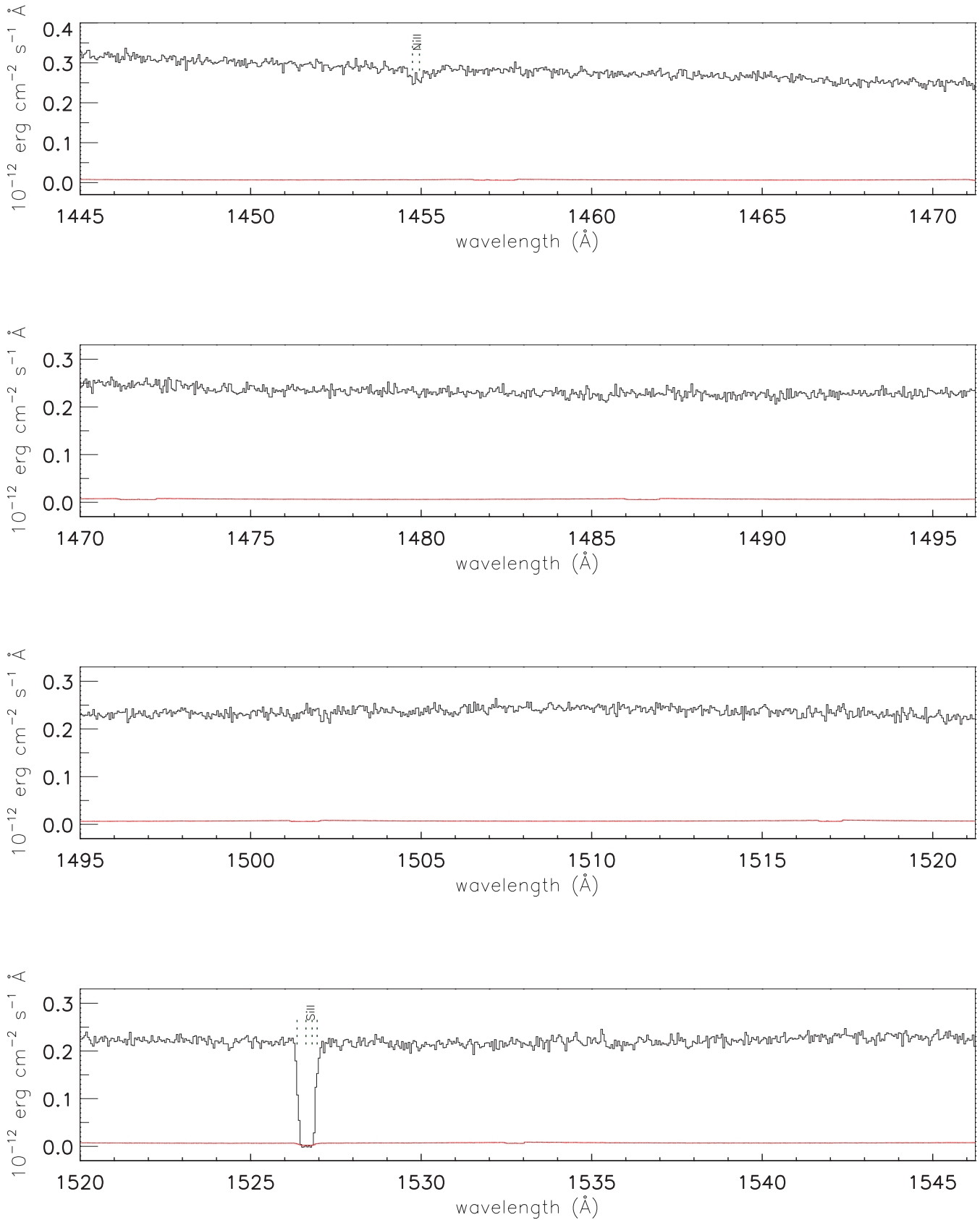


Figure 1 – *continued*

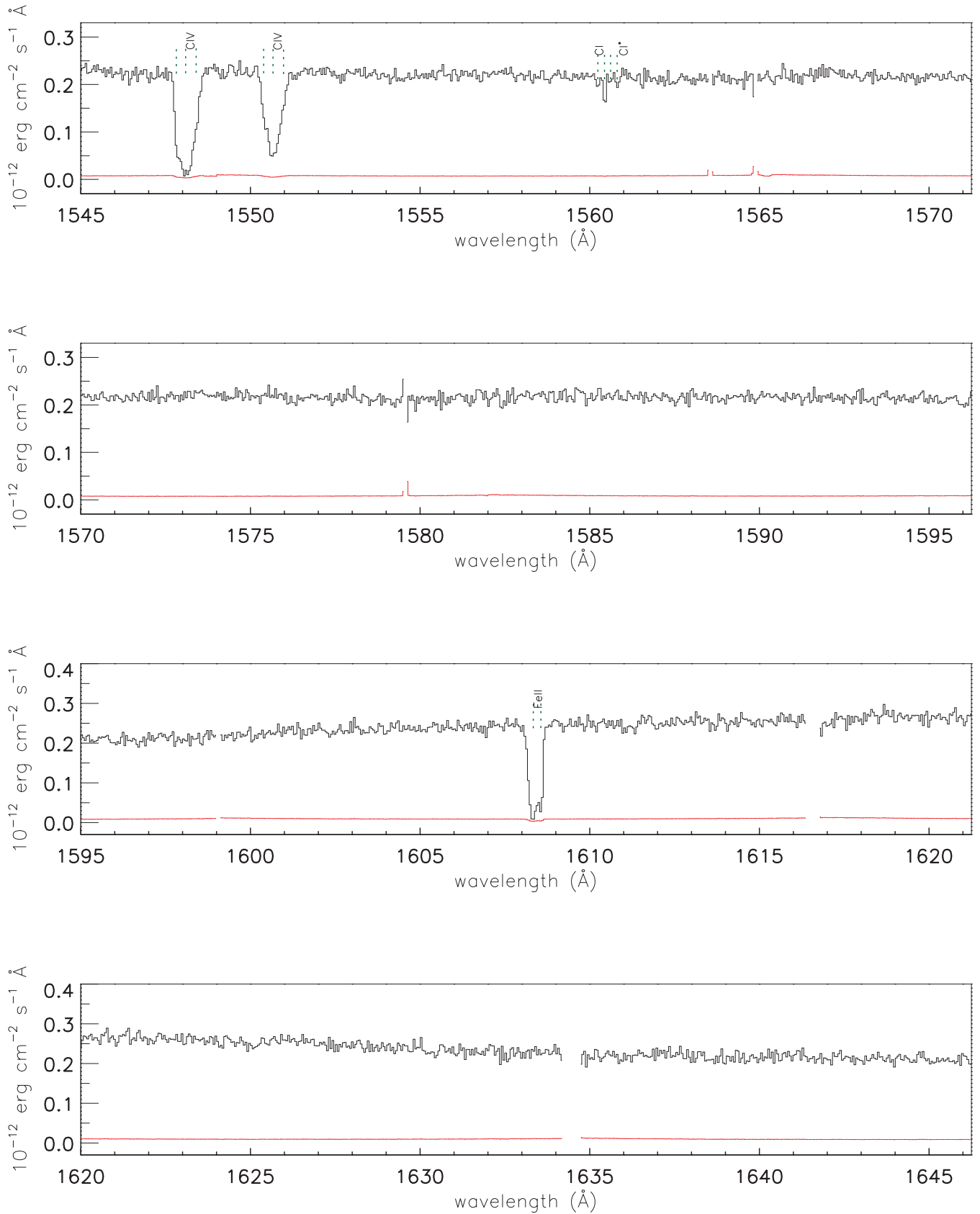
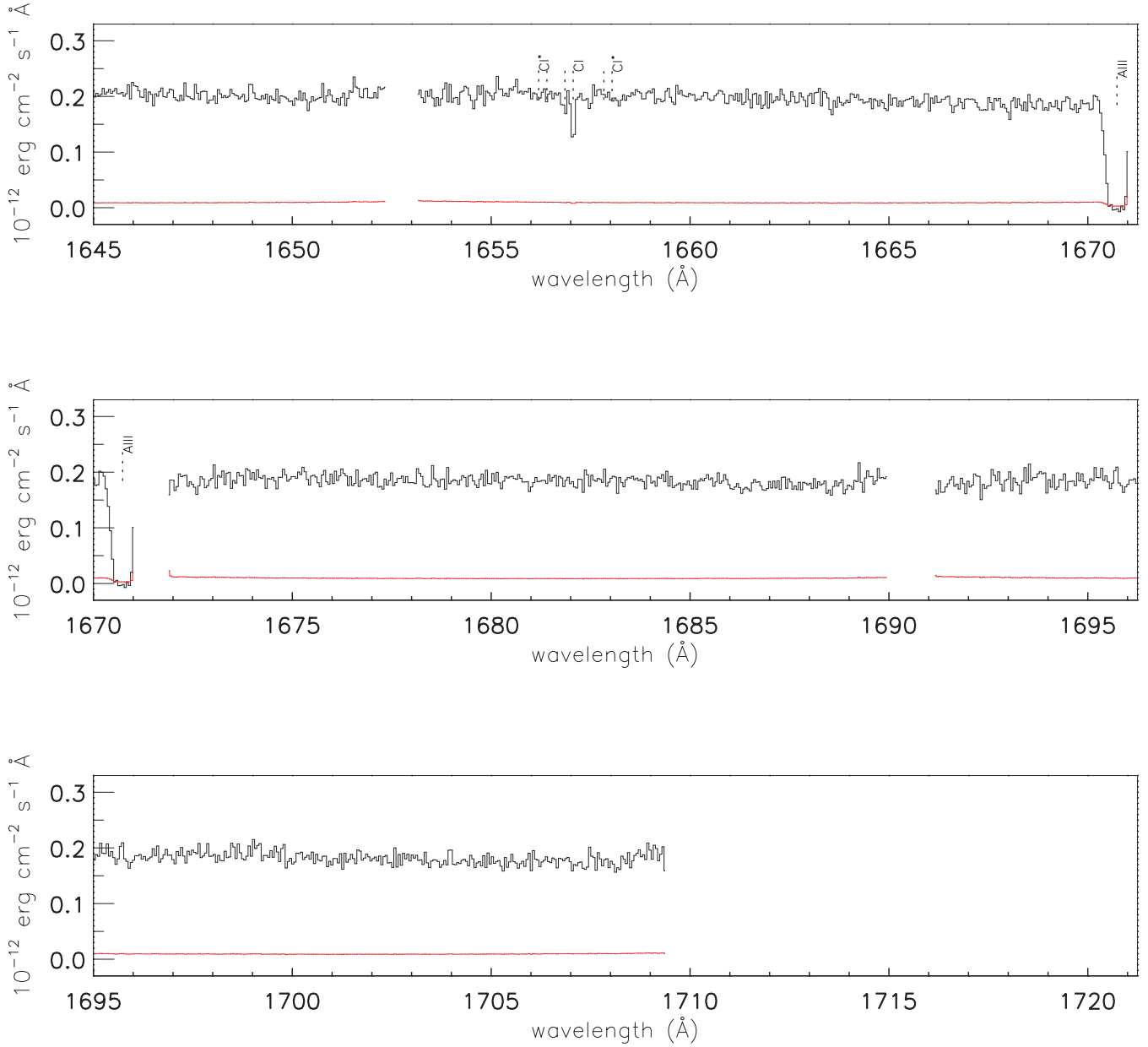


Figure 1 – continued

Figure 1 – *continued***Table 1.** Statistics of simulated data: Doppler parameters.

S/N ^a	Doppler parameter (km s ⁻¹)		Doppler parameter (km s ⁻¹)		Doppler parameter (km s ⁻¹)	
	input ^b	recovered ^c	input ^b	recovered ^c	input ^b	recovered ^c
20	17.2 ≤ <i>b</i> ≤ 17.8	19.0 ± 5.0(4.1)	22.2 ± 5.5	21.8 ± 8.0(5.5)	35.0 ± 0.6	35.3 ± 8.1(8.1)
40	17.2 ≤ <i>b</i> ≤ 17.8	19.5 ± 6.8(4.5)	24.7 ± 0.1	26.7 ± 7.0(6.3)	35.0 ± 0.6	35.0 ± 7.0(7.2)

^aS/N per pixel in simulated STIS spectra.

^bMean and first order about the mean for input Doppler parameters in simulations which were recovered. The simulations for S/N = 20, $\langle b \rangle = 22.2 \text{ km s}^{-1}$, were made from a distribution made at the beginning of our analysis, with a much wider standard deviation (5.5 km s^{-1}) in input *b* than the others, hence the difference with the $\langle b \rangle = 24.4 \text{ km s}^{-1}$ case (the geometric mean of 17.5 and 35.0). The results between the two cases agree within the errors, so we did not make a simulation run with S/N = 20, $\langle b \rangle = 24.7 \text{ km s}^{-1}$.

^cMean and first order about the mean for recovered Doppler parameters in simulations, with the mean in the formal 1σ profile fitting errors in parentheses. The mean recovered Doppler parameters are all within the mean profile fitting errors of the input values.

Table 2. Statistics of simulated data: H I column densities.

S/N ^a	Doppler ^b parameter (km s ⁻¹)	log N(H I)	
		input ^c	recovered ^d
20	17.5	12.54 ± 0.12	12.55 ± 0.12(0.07)
40	17.5	12.17 ± 0.12	12.20 ± 0.11(0.09)
20	22.2	12.41 ± 0.10	12.41 ± 0.13(0.08)
40	24.7	12.26 ± 0.12	12.28 ± 0.13(0.08)
20	35.0	12.64 ± 0.12	12.65 ± 0.13(0.08)
40	35.0	12.36 ± 0.12	12.37 ± 0.13(0.07)

^aS/N per pixel in simulated STIS spectrum.

^bSimulation sets are specified by input Doppler parameter.

^cMean and first order about the mean for input log H I column densities in simulations which were recovered.

^dMean and first order about the mean for recovered log H I column densities in simulations, with the mean in the formal 1 σ profile fitting errors in parentheses.

lines narrower presumably would cause the features to drop below the (essentially equivalent width-defined) detection threshold (Rauch et al. 1993). The recovery of the line parameters (e.g. the b -value) was found to be even better for stronger lines detected at high significance, up until the point where the H I lines start to saturate badly. The spurious detection rate is <1 per cent among all the simulations above the 80 per cent detection probability threshold, and thus is not considered significant. The boundary of the 80 per cent detection probability threshold can be parametrically fitted by $\log N_{\text{H I}} = 12.11 + 0.27 \log(b/24.7) - 1.12 \log(\text{snr}/40.)$, where snr is the signal-to-noise ratio (S/N) per pixel, and established using simulated lines with $16 \lesssim b \lesssim 36 \text{ km s}^{-1}$. The process was adapted from the method used in Paper I.^{2,3} We consider this parametrization useful to determine our 80 per cent detection threshold over a Doppler parameter range of 10–40 km s⁻¹, with the bounds based both on our simulations and to compare with the analysis of Lehner et al. (2007a).

3.4 Profile fits to data

In addition to H I lines, we find and list, for completeness, profile fits or column density limits (from VPFIT or from the apparent optical depth method, Savage & Sembach 1991) for a number of Galactic and intervening metal absorber species.

² The coefficient of 0.27 for $\log(b/24.7)$ for this paper is ~ 25 per cent lower than the analogous value of 0.34 from Paper I, and the snr coefficient in this work is 11 per cent higher. The difference in the $\log(b/24.7)$ coefficient may be caused by the relatively lower column density range used for the input lines for this study, in that the limited Doppler parameter range used affects the equivalent widths and thus detectability of the lines less strongly. The difference in the snr coefficient may also stem from a similar cause, or from either the higher S/N in the 3C 273 data and/or the use of only two input S/N values in this study, 20 and 40. In comparison, for PKS 0405–123, we used three evenly distributed in log space over the range we tested. The difference in results between a coefficient of 1.12 and 1.00 (without adjusting the other coefficients) is only 0.03 dex for our minimum S/N of 21, and the current value of 1.12 leads to a more conservative detection threshold as $\text{snr}/40 < 1$. We do not believe that the results of this paper are significantly affected by the difference in parametrization.

³ We will publish an erratum for Paper I (Williger et al., in preparation). In that paper, a subset of absorbers principally below the 80 per cent detection threshold had erroneously high calculated significance because the contribution of continuum uncertainties to the total equivalent width errors was not included in the software.

Galactic absorption. We find Galactic absorption from H I, C I, C I*, C II, C II*, C IV; N I, N V, O I, Mg II, Al II, Si II, Si III, Si IV, P II, S II, S III, Mn II, Fe II and Ni II. Galactic absorption ranges over $-135 < v < 68 \text{ km s}^{-1}$, consistent with the high velocity absorption found in the *FUSE* spectrum by Sembach et al. (2001). A complete list of absorber profile fitting parameters is in Table 3. In the case of saturated lines, we calculate lower limits by the apparent optical depth method Savage & Sembach (1991), which are consistent with the results of Sembach et al. (2001). The maximum optical depth used is a function of local S/N and continuum error $\{\tau_{\text{max}} \sim \ln[\sqrt{2}/(S/N)] \text{ per pixel}\}$, in which both effects contribute to similar degrees. For the 3C 273 data, $\tau_{\text{max}} \sim 2.3\text{--}3.0$.

For two of the highest $N_{\text{H I}}$ column density systems towards 3C 273, members of this collaboration and others have investigated metallicity limits and undertaken studies in the low- z IGM (e.g. Davé et al. 2001; Tripp et al. 2002; Stocke et al. 2007; Tripp et al. 2008). Such low redshift, high column density absorbers are extremely useful for comparison with nearby low luminosity faint galaxies e.g. the dwarf galaxy found 71 kpc away from the $z = 0.0053$ Virgo cluster absorber (Stocke et al. 2004). For completeness and comparison with their results, we provide here upper limits for C IV for each of these $N_{\text{H I}}$ absorbers, and for a sum of the C IV regions over a consistent $-100 \leq \Delta v \leq 100 \text{ km s}^{-1}$, using the above-mentioned apparent optical depth method. The $z = 0.003369$ absorber was found by Tripp et al. to have rest equivalent width $W_{r,\text{C IV}} < 27 \text{ mÅ}$ over $-100 < \Delta v < 100 \text{ km s}^{-1}$ or $\log N(\text{C IV}) < 12.8$ assuming an absorber on the linear part of the curve of growth. Stocke et al. found $\log N(\text{C IV}) < 12.27$ (3σ) for the $z = 0.066548$ system over $-50 < \Delta v < 50 \text{ km s}^{-1}$. We measured an upper limit for the $z = 0.066548$ absorber of $W_{r,\text{C IV}} \lesssim 50 \text{ mÅ}$ (3σ) over $-100 < \Delta v < 100 \text{ km s}^{-1}$ or $\log N(\text{C IV}) \lesssim 13.1$.⁴ We stacked the data for the two systems and found $W_{r,\text{C IV}} \lesssim 19 \text{ mÅ}$ (3σ) $-100 < \Delta v < 100 \text{ km s}^{-1}$ or $\log N(\text{C IV}) \lesssim 12.7$.⁵

4 RESULTS AND DISCUSSION

4.1 Ly α absorber statistics

We use our detection probability results to define a sample for $\log[N(\text{H I})] \geq 12.5$, which is approximately the 80 per cent detection threshold for our worst case S/N = 20 in the Ly α forest and assuming a Doppler parameter of $b = 40 \text{ km s}^{-1}$.⁶ This low H I column density threshold sample covers the range $0.020 < z < 0.139$ and contains 21 Ly α absorbers. We excluded absorbers within $\Delta v \sim 5000 \text{ km s}^{-1}$ of 3C 273 to minimize the impact of the proximity effect (Murdoch et al. 1986; Bajtlik, Duncan & Ostriker 1988).

⁴ The difference in upper limits arises in that the Stocke et al. limit is for one resolution element, whereas our limit is over 200 km s^{-1} in velocity space or ~ 28 resolution elements, to be consistent with the Tripp et al. measurement.

⁵ This limit is slightly tighter than the 24 mÅ result expected from stacking the spectra according to the inverse square of the S/N. The difference in our result may be from the way each team determined the local continuum and S/N, in particular as these were measured over two different velocity intervals.

⁶ Note that by choosing $b = 40 \text{ km s}^{-1}$, this leads to a higher, more conservative 80 per cent probability detection threshold in $N_{\text{H I}}$ by 0.06 dex than by choosing $b = 25 \text{ km s}^{-1}$, which is typical of high resolution, high S/N Ly α forest data. We prefer to be conservative, given the possibility of unresolved blends caused by our limits in the achievable S/N. This choice of b does not affect our subsequent analysis in any way except for this small change in the threshold for $\log N_{\text{H I}}$.

Table 3. Galactic absorption lines towards 3C 273 from STIS data.

Species	z	Error ^a	b (km s ⁻¹)	Error ^a	$\log N$ (km s ⁻¹)	Error ^a	Lines (Å) ^{c,f,g}
O I	-0.000451	0.000041	61.5	22.1	13.55	0.12	1302
C IV	-0.000240	0.000003	11.6	1.8	13.45	0.09	1548,1550
Si IV	-0.000230	0.000003	7.9	1.4	12.57	0.06	1393,1402
Si II	-0.000224	>13.24	...	1190,1193,1260,1304,1526
O I	-0.000220	>13.59	...	1302
S II	-0.000159	0.000016	10.1	4.9	13.74	0.24	1250,1253,1259
Si IV	-0.000103	>13.19	...	1393,1402
S III	-0.000084	>14.26	...	1190
Fe II	-0.000071	>14.71	...	1608
N I	-0.000067	>15.04	...	1199,λλ1200
Mn II	-0.000067	...	14.2	...	12.60	0.19	1197,1199,1201 ^d
Ni II	-0.000067	0.000004	22.3	1.7	13.73	0.03	1317,1370,1454
C II	-0.000067	>15.54	...	1334
C IV	-0.000066	0.000003	>14.46	...	1548,1550
S II	-0.000060	>15.22	...	1250,1253,1259
Si IV	-0.000060	0.000012	48.8	2.3	13.73	0.04	1393,1402
P II	-0.000056	0.000017	29.1	7.5	13.69	0.10	1152,1532
Si II	-0.000067	>15.03	...	1190,1193,1260,1304,1526
C II*	-0.000045	0.000002	14.3	0.8	13.83	0.02	1335
C I*	-0.000044	0.000000	9.1	0.0	12.24	0.26	1561,1656,1657 ^e
C I	-0.000044	0.000005	9.1	2.4	12.79	0.07	1277,1280,1328,1560,1656
Si III	-0.000042	>14.02	...	1206
Mg II	-0.000038	0.000012	27.9	5.1	15.43	0.06	1239,1240
N V	-0.000037	0.000005	59.8	2.2	13.93	0.01	1238,1242
Al II	-0.000033	>13.62	...	1670
H I	-0.000027	0.000005	20.23	0.00	Lyα, β
O I	-0.000025	>15.38	...	1302
Fe II	0.000068	>14.28	...	1608
N I	0.000068	>14.66	...	1199,λλ1200
Mn II	0.000068	...	4.4	...	12.63	0.18	1199,λλ1200 ^d
S II	0.000069	0.000001	9.4	0.6	14.75	0.01	1250,1253,1259
Ni II	0.000074	0.000004	13.3	2.0	13.41	0.05	1317,1370
C II*	0.000078	0.000001	7.6	0.7	13.73	0.02	1335
C I	0.000081	0.000001	6.4	0.7	13.27	0.02	1277,1280,1328,1560,1656
C I*	0.000081	0.000000	6.4	0.0	12.67	0.09	1561,1656,1657 ^e
C IV	0.000138	0.000012	20.7	4.4	13.32	0.15	1548,1550
Si II	0.000159	>14.59	...	1190,1193,1260,1304,1526
S II	0.000171	0.000009	1.3	4.1	13.13	0.21	1250,1253,1259
O I	0.000190	0.000015	13.0	5.7	13.41	0.19	1302
C II	0.000206	>14.89	...	1334
Si IV	0.000225	0.000020	15.2	11.6	12.21	0.56	1393

^aErrors are 1σ , and assume that the component structure is correct.

^bUpper limits from v_{FIT} or the apparent optical depth method of Savage & Sembach (1991).

^cLines used in profile fits.

^dMn II tied in redshift and Doppler parameter to N I.

^eC I* tied in redshift and Doppler parameter to C I.

^fWe find an unidentified feature at 1149.3 Å (also in the *FUSE* data).

^gWe find a weak feature at 1304.74 Å to be an artefact just redward of an echelle overlap region, and not securely identifiable with any plausible ISM or IGM absorption.

In later sections, we will discuss in detail our examinations of the Ly α forest Doppler parameter distribution, redshift density dN/dz , broad line population and column density distribution. We do not distinguish between metal and Ly α -only systems in this analysis, the same approach as in Paper I. Metals have been found in progressively lower column density Ly α systems at $z \gtrsim 2$ (e.g. Cowie et al. 1995; Songaila & Cowie 1996; Pettini et al. 2001, and references therein). Also, the absorbers we can detect at low redshift probably are best related to large density perturbations at $z \gtrsim 2$ (e.g. Schaye 2001) which are commonly associated with metals. Finally, the limited wavelength range of the data does not permit a uniform coverage for metal detection (in particular for C IV, limited to $z \lesssim 0.1$).

4.1.1 Redshift density and intervening absorber list

Measuring the Ly α forest redshift density has been one of the biggest goals among *HST* key projects, and initially yielded surprising results. From among the first results with Faint Object Spectrograph (FOS) Bahcall et al. (1991) and GHRS Morris et al. (1991) towards 3C 273, the Ly α redshift density was found to be higher than expected from extrapolations of ground-based data. To compare results with recent high-resolution data in the literature, we present data for $13.1 \leq \log N_{\text{H I}} < 14.0$ and $14.0 \leq \log N_{\text{H I}} < 17.0$, using the restrictions of $b \leq 40 \text{ km s}^{-1}$, and errors in b and $N_{\text{H I}}$ of ≤ 40 per cent for both 3C 273 and the literature values (to use the same criteria as Lehner et al. 2007a). We also present results for

Table 4. Intervening absorption lines towards 3C 273 from STIS data.

Species	z	Error ^a	b (km s ⁻¹)	Error ^a	log N	Error ^a	Lines (Å) ^{b,c}
H I	0.002630	0.000039	125.8	44.9	13.04	0.14	Ly α
H I	0.003369	0.000002	37.4	0.8	14.22	0.02	Ly α , β^e
H I	0.005251	0.000021	26.1	1.3	14.33	0.31	Ly α , β^e
Si II	0.005266	0.000005	5.2	2.6	11.78	0.09	1190,1260
H I	0.005295	...	15.0	0.0	15.68	0.04	Ly α , β , γ , δ , ϵ , ζ , θ , κ^e
C II	0.005295	...	8.6	0.1	12.80	0.07	1036,1334
Si III	0.005295	0.000002	8.2	2.1	12.36	0.07	1206, sets z for Si III, H I
H I	0.007165	0.000029	38.8	12.1	12.67	0.12	Ly α
H I	0.007588	0.000037	64.0	18.0	12.86	0.10	Ly α
H I	0.026225	0.000006	26.7	2.5	12.95	0.03	Ly α
H I	0.029348	0.000028	17.1	6.4	12.77	0.28	Ly α
H I	0.029471	0.000008	19.7	7.8	13.24	0.16	Ly $\alpha^{d,e}$
H I	0.029578	0.000016	11.6	5.9	12.63	0.30	Ly α
H I	0.032798	0.000006	22.8	2.6	12.82	0.04	Ly α
H I	0.039373	0.000012	28.2	5.2	12.63	0.06	Ly α
H I	0.046639	0.000013	24.4	5.5	12.51	0.08	Ly α
H I	0.049000	0.000002	28.7	0.7	13.56	0.01	Ly $\alpha^{d,e}$
H I	0.049953	0.000004	16.2	1.7	12.83	0.03	Ly α
H I	0.054399	0.000017	23.6	6.6	12.41	0.10	Ly α
H I	0.063510	0.000018	17.9	3.9	12.96	0.14	Ly α
H I	0.064078	0.000025	39.8	10.9	12.62	0.09	Ly α
H I	0.066548	0.000001	36.7	0.5	14.08	0.01	Ly α , β^e
H I	0.073738	0.000034	64.0	15.0	12.74	0.08	Ly α
H I	0.074286	0.000033	51.2	13.8	12.62	0.10	Ly α
H I	0.075377	0.000009	27.1	3.8	12.77	0.05	Ly α
H I	0.085882	0.000028	34.9	11.3	12.41	0.11	Ly α
H I	0.087632	0.000008	43.3	3.1	13.09	0.03	Ly α
H I	0.089746	0.000012	30.5	4.4	13.08	0.06	Ly α
H I	0.089898	0.000009	12.8	4.3	12.60	0.15	Ly α
H I	0.090110	0.000004	30.1	1.8	13.29	0.02	Ly $\alpha^{d,e}$
H I	0.109141	0.000015	18.8	6.2	12.33	0.11	Ly α
H I	0.109380	0.000009	18.7	3.8	12.56	0.06	Ly α
O VI	0.12003	13.45	0.10	1032,1038 ^f
H I	0.120041	0.000002	21.5	0.7	13.50	0.01	Ly $\alpha^{d,e}$
H I	0.141676	0.000024	32.6	9.6	12.36	0.10	Ly α
H I	0.146575	0.000005	39.0	1.7	14.08	0.03	Ly α , β^e
H I	0.150204	0.000021	32.9	7.8	12.37	0.08	Ly α
H I	0.157787	0.000006	21.5	2.1	12.63	0.03	Ly α
O VI	0.15779	13.39	0.11	1032 ^f

^aErrors are 1σ , and assume that the component structure is correct.

^bLines used in profile fits.

^cWe find an unidentified feature at 1149.3 Å (also in the *FUSE* data).

^dInclusion of Ly β makes no significant difference to the fit.

^eLy α absorption confirmed by Ly β .

^fTripp et al. (2008).

$\log N_{\text{H I}} \geq 12.5$. Due to the low redshift of 3C 273, the data are unaffected by losses of interorder gaps in the STIS data. Similar to our analysis in Paper I, we excluded pixels from metal absorption with optical depth $\tau \geq 2$, which removed $\Delta z = 0.002$ from the samples for $\log N_{\text{H I}} \geq 13.1$ and $\log N_{\text{H I}} \geq 14.0$.⁷ This left an unblocked redshift path of $\Delta z = 0.135$ for $\log N_{\text{H I}} \geq 13.1$ and for $\log N_{\text{H I}} \geq 14.0$. In an analogous way, we find $\Delta z = 0.117$ for

⁷ Metal absorption from pixels with $\tau < 2$ can also reduce the probability of detection an IGM Ly α absorber, but less so than those with $\tau \geq 2$. The value of $\tau = 2$ is a compromise to eliminate the worst metal absorption regions without losing too many pixels with recoverable Ly α data. Other factors such as multiple transitions from a metal ion can mitigate the masking effect of metal absorption. For example, we recovered the presence of Ly α absorption blended with Galactic Si IV.

$\log N_{\text{H I}} \geq 12.5$ (which requires a smaller, higher S/N subset of the data). The absorption distance $\Delta X = 0.124$ (Tytler 1987), using the prescription of Lehner et al. (2007a), which will be used for comparing H I column density distributions in the next section.

We list in Table 4 intervening H I and related metal redshifts, column densities and Doppler parameters, including several systems either outside of the unblocked redshift intervals corresponding to the sensitivities mentioned above, or at $12.3 \leq \log N_{\text{H I}} < 12.5$ which nevertheless fulfill all of the other selection criteria. We show in Fig. 2 the Doppler parameters and H I and column densities for all Ly α forest systems that we detected using the procedure described in Section 3, overlaid with the our parametrically fitted 80 per cent detection sensitivities.

(A) *High column density lines* $\log N_{\text{H I}} \geq 14.0$. For absorbers with $\log N_{\text{H I}} \geq 14.0$ from among our full sample of 21 systems, we find four over the interval $0.002 < z < 0.139$ ($\log dN/dz = 1.47_{-0.30}^{+0.18}$).

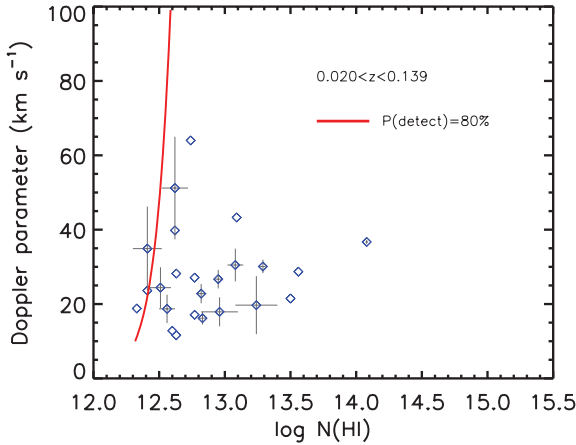


Figure 2. H I column densities and Doppler parameters. Ly α forest sample over $0.020 < z < 0.139$, which is the redshift range used for our sample of $\log N_{\text{HI}} \geq 12.5$. Open diamonds: data points. For clarity, only error bars for every second point are shown. The line indicates the parametric approximation to the 80 per cent detection probability from simulations in Section 3.4, based on $S/N \geq 21$. Three absorbers with $12.3 \leq \log N_{\text{HI}} \leq 12.5$ used for column density studies are also included.

If we restrict our sample to $b \leq 40 \text{ km s}^{-1}$ and errors in b and N_{HI} to ≤ 40 per cent, the number reduces to three ($\log dN/dz = 1.35^{+0.19}_{-0.38}$). The difference arises from the lower N_{HI} component of the $z = 0.0053$ Virgo absorber, which has a column density error of a factor of 2 and is examined in more detail in Section 4.4. We compare our results with the literature (Fig. 3), and illustrate the scatter for seven other sightlines with contiguous redshift coverage of $\Delta z > 0.13$ from Paper I (PKS 0405–123, $\Delta z = 0.413$),⁸ Sembach et al. (2004, PKS1116+215, $\Delta z = 0.133$), Richter et al. (2004, PG 1259+593, $\Delta z = 0.247$), Lehner et al. (2007a, HE0226–4110, H1821+643 and PG0953+415, $\Delta z = 0.397, 0.238, 0.202$, respectively) and Aracil et al. (2006, HS 0624+6907, $\Delta z = 0.329$). The redshift density is marginally high (similar to PKS 0405–123) but still consistent with other measurements from the literature shown in Fig. 3 (right-hand panel), similarly selected for $b \leq 40 \text{ km s}^{-1}$ and with errors in b and N_{HI} of ≤ 40 per cent. The small number statistics and large cosmic scatter (~ 0.7 dex in dN/dz for individual sightlines) make further analysis difficult without larger samples. The cosmic scatter range appears to persist to $z \sim 1$. To illustrate the effect of the restriction in b and in the errors, we also included the redshift density from the large, lower resolution sample of Weymann et al. (1998), which was selected on the basis of rest equivalent width and cannot filter out $b > 40 \text{ km s}^{-1}$ systems, and is $\sim 1\sigma$ higher than our result. We note that the $z \approx 0$ dN/dz determination of Wakker & Savage (2009) is consistent with the Weymann et al. result, as both studies relied on equivalent widths rather than column densities with restrictions on the Doppler parameters. The redshift densities for restricted, high resolution $z \lesssim 0.3$ sightlines are in general a factor of ~ 2 – 3 lower than the analogous $1 < z < 2$ sightlines.

(B) *Medium column density lines* $13.1 \leq \log N_{\text{HI}} < 14.0$. In both of our full sample and restricted sample for $b \leq 40 \text{ km s}^{-1}$ and errors in b and N_{HI} of ≤ 40 per cent, we find four absorbers over the interval $0.002 < z < 0.139$ with $13.1 \leq \log N_{\text{HI}} < 14.0$ ($\log dN/dz = 1.47^{+0.18}_{-0.30}$). We compare our results with the literature, and illustrate the scatter for seven other sightlines with contiguous

redshift coverage of $\Delta z > 0.13$ from Paper I (PKS 0405–123, $\Delta z = 0.212$), Sembach et al. (2004, PKS1116+215, $\Delta z = 0.133$), Richter et al. (2004, PG 1259+593, $\Delta z = 0.247$), Lehner et al. (2007a, HE0226–4110, H1821+643 and PG0953+415, $\Delta z = 0.294, 0.238$ and 0.202 , respectively) and Aracil et al. (2006, HS 0624+6907, $\Delta z = 0.329$). We note that Lehner et al. estimated completeness to $\log N_{\text{HI}} = 13.2$, so the line densities for the three objects from that study should be a lower limit. For PKS 0405–123, we use a revised line list for PKS 0405–123 (Williger et al., in preparation) and the redshift interval known to be complete to $\log N_{\text{HI}} = 13.1$ (Paper I). We consulted with N. Lehner about the S/N characteristics of the other sightlines in their work (private communication). We have split the HS 0624+6907 sightline into high and low z halves to keep the redshift intervals to similar length compared to that of 3C 273. Results are plotted in Fig. 3 (left-hand panel).

The cosmic scatter covers about 0.2 dex in dN/dz at $z \lesssim 0.3$, for all sightlines except 3C 273, which is $\sim 1.5\sigma$ below the mean of the other seven sightlines. For comparison, the $z \approx 0$ redshift density of Wakker & Savage of $\log dN/dz \sim 2 \pm 0.1$ [based on their fig. 5(b)] is just consistent with the maximum of the individual sightline values, again possibly showing the difference in redshift density using equivalent widths versus column densities with restricted Doppler parameters. At $z \sim 1$, a larger sample (Janknecht et al. 2006) indicates a cosmic scatter range of 0.35 dex which spans both the 3C 273 value and the other seven low- z sightlines, so the 3C 273 sightline may simply represent the lower end of the redshift density range. The high signal and high resolution in the data here make it unlikely that blending and noise effects are mainly responsible for the paucity of Ly α forest lines towards 3C 273 in this column density range. The Cosmic Origins Spectrograph should reveal more definitively whether $\log dN/dz \approx 1.5$ is a representative of one of the sparsest parts of the Ly α forest, or if even more poorly populated sightlines exist.

(C) *Low column density lines* $\log N_{\text{HI}} \geq 12.5$. Given the very high S/N in the 3C 273 data, we also calculate the redshift density for $\log N_{\text{HI}} \geq 12.5$. We find 21 absorbers above this threshold over $0.020 < z < 0.139$, for $\log dN/dz = 2.25^{+0.09}_{-0.10}$. To compare the 3C 273 sample to the much larger observational data set of Lehner et al. (2007a), we consider separately those systems with errors in Doppler parameter and N_{HI} under 40 per cent (based on the lower limit 1σ errors for N_{HI}) and $b < 40 \text{ km s}^{-1}$. These criteria focus the sample on relatively cool IGM gas by excluding broad Ly α systems (BLAs; e.g. Richter et al. 2006a,b), which are interpreted as the signatures of physically distinct low- z hot IGM gas. The restricted 3C 273 sample is 18 systems ($\log dN/dz = 2.19^{+0.10}_{-0.12}$), which consistent to 1σ in redshift density with the full sample.

There are few comparisons down to a threshold of $\log N_{\text{HI}} \geq 12.5$ for absorbers at low z . Observationally, Danforth & Shull (2008) found $\log dN/dz \sim 1.5^{+0.2}_{-0.1}$ for $z < 0.4$ (see their fig. 3), which is 2 – 3σ below our value of $\log dN/dz = 2.19^{+0.10}_{-0.12}$, and Wakker & Savage (2009) determined $\log dN/dz \sim 2.4 \pm 0.2$ for $z \approx 0$, which is consistent with our value. These results could be understood in that the weakest lines in the sample dominate the number counts, based on the column density distribution, and should affect an equivalent width based sample (such as Wakker & Savage) less than a sample with a higher column density floor of $\log N_{\text{HI}} = 13.1$. From numerical models, Paschos et al. (2009) calculated $\log dN/dz \approx 2.1$ for the same H I threshold at $z = 0.1$, which is consistent with our measurements to 1 – 1.5σ . Less directly, at $z = 0$, our H I column density threshold corresponds to

⁸ We corrected the line list for spurious absorbers, and will publish the updated list in an erratum (Williger et al., in preparation).

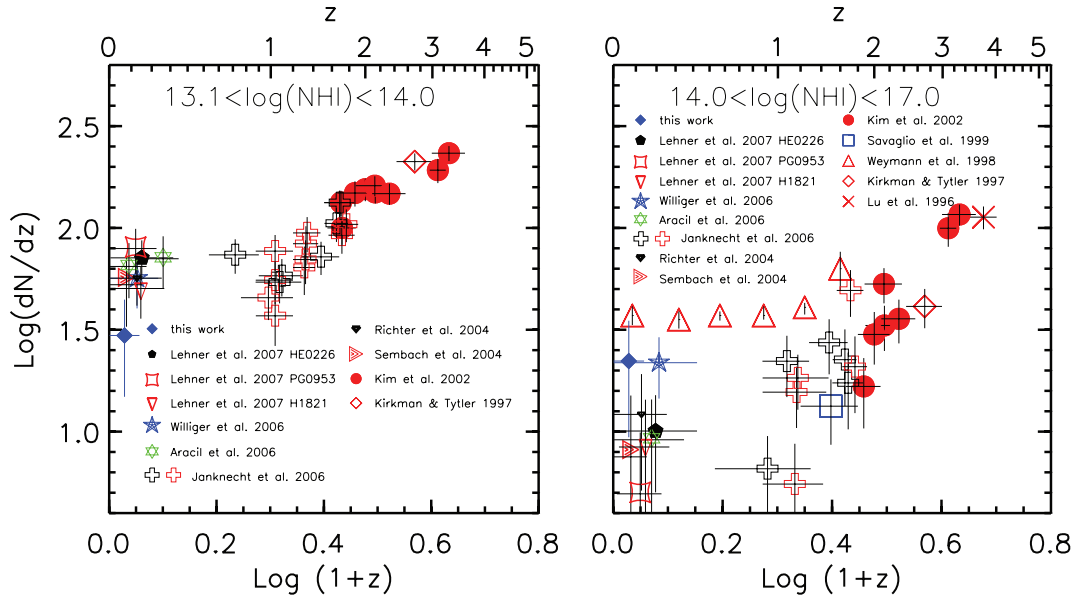


Figure 3. Left-hand panel: Ly α forest redshift density dN/dz for $13.1 < \log N_{\text{HI}} < 14.0$. Right-hand panel: $14.0 < \log N_{\text{HI}} < 17.0$. Error bars show redshift bins and Poissonian errors in dN/dz . We restrict the data to $b \leq 40 \text{ km s}^{-1}$, and to errors in b and N_{HI} of ≤ 40 per cent for 3C 273 and the literature values in both cases except for the Weymann et al. (1998) values, which are based on equivalent widths and are shown for comparison. For the open crosses of Janknecht et al. (2006), dark symbols denote the highest quality data and light (red) symbols all data, as defined in Section 4.2 of Lehner et al. (2007a).

overdensities of $\log(\rho_{\text{H}}/\bar{\rho}_{\text{H}}) \sim 0.4 \pm 0.2$ (Davé et al. 1999; Davé & Tripp 2001) as calculated from hydrodynamical models in the CDM scenario. At $z \sim 3$, the same overdensity level corresponds to $\log N_{\text{HI}} \sim 14.0\text{--}14.5$, a rough estimate for which can be read from the right-hand panel of Fig. 3: $dN/dz \approx 2.2 \pm \sim 0.1$. Our results are therefore consistent with overdensities of $\log(\rho_{\text{H}}/\bar{\rho}_{\text{H}}) \sim 0.4 \pm 0.2$ within 1.1σ . We caution that the correspondence of overdensity and dN/dz may only result from the considered density perturbations being weak, as non-linear growth would be expected over time to skew the overdensity distribution to high values; the low- z IGM is relatively complex, containing a significant fraction of shock-heated gas (which is related to the BLA population).

The observation of many more sightlines with COS would likely reveal better the extent of cosmic scatter, and provide further comparisons between the Ly α forest and galaxy environments e.g. Chen et al. (2005). In particular, COS could provide a large increase in sightlines probed to $\log N_{\text{HI}} \sim 12.5$, though at lower resolution than this study.

4.1.2 Doppler parameter distribution

The Doppler parameter distribution for the entire sample of 21 absorbers has mean, median and standard deviation of 28, 27, 13 km s^{-1} , respectively (Fig. 4). In the same manner as Paper I, we tested whether weak line blending is the cause. We divided the strong sample into high and low H I column density halves, which occurs at $\log N_{\text{HI}} = 12.80$, and performed a Kolmogorov–Smirnov test to determine the likelihood that the Doppler parameters are drawn from the same distribution. The probability that the samples are drawn from the same distribution is $P = 0.96$. The closest observed Ly α forest absorber pair in velocity space is $\Delta v = 31 \text{ km s}^{-1}$ (between $z = 0.029471, 0.029578$) or 4–5 times the resolution of the STIS data. The next closest pair is $\Delta v = 41 \text{ km s}^{-1}$. This can be compared to the mean velocity interval expected between absorbers (in the absence of clustering, which is expected to be weak and shows no evidence to the contrary, Section 4.3) of $\langle \Delta v \rangle \sim 1500\text{--}$

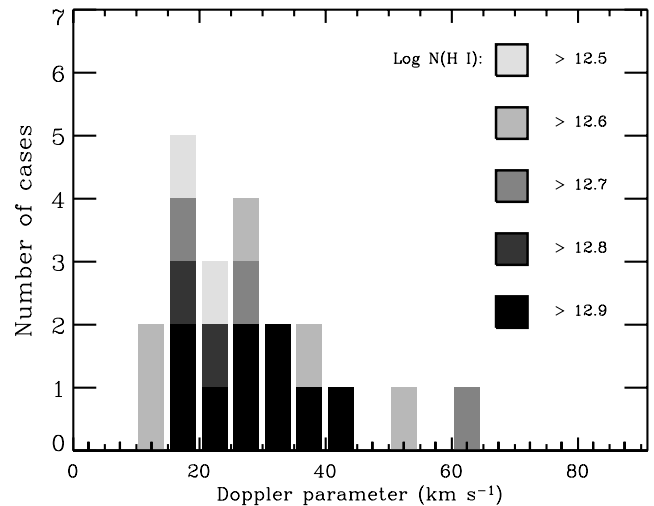


Figure 4. Ly α Doppler parameter distribution for a series of minimum $\log N_{\text{HI}}$ thresholds in the complete sample.

1700 km s^{-1} , based on our value of dN/dz for $\log N_{\text{HI}} \geq 12.5$ over $0.020 < z < 0.139$. We would then expect to first approximation that there is a ~ 0.5 per cent chance of an absorber randomly being $\sim 8\text{--}9 \text{ km s}^{-1}$ from another. At such a velocity difference, the lines could potentially be unresolved, depending on the local S/N and the line column densities and Doppler parameters, with the greatest possibility of blending for broad, shallow lines in relatively noisy parts of the data. For the high S/N in the 3C 273 data and the $b < 40 \text{ km s}^{-1}$ absorbers with < 40 per cent errors upon which we are focused, we infer that line blending is not significant for the Ly α forest towards 3C 273.

We compared results with the much larger low- z sample of Lehner et al. (2007a). They restricted their sample to $b < 40 \text{ km s}^{-1}$, to correct for the non-Gaussianity of the Doppler parameter distribution. If we make the same restriction for our data, the sample would have

18 absorbers, with mean, median and standard deviation 24, 24 and 8 km s^{-1} . Lehner et al. (2007a) found values of 27, 27 and 8 km s^{-1} , which is consistent with our results. The $\log \gtrsim 13.7$, $z < 0.23$ sample of Shull et al. (2000) is also consistent (mean, median and standard deviation 31, 28 and 7 km s^{-1} respectively). Finally, our $b < 40 \text{ km s}^{-1}$ sample is in accord with the Doppler parameter mean of Davé & Tripp (2001) (25 km s^{-1}), which is complete for $\log N_{\text{HI}} \geq 13.0$ and includes absorbers down to $\log N_{\text{HI}} = 12.6$, and thus shows agreement with their comparison model of a Λ -dominated CDM universe (Davé et al. 1999), and again with the more recent simulations of Paschos et al. (2009).

4.1.3 Column density distribution

Observations suggest (e.g. Kim et al. 2002; Misawa et al. 2007) and simulations predict (e.g. Paschos et al. 2009) that the column density distribution should steepen at lower redshift for $\log N_{\text{HI}} \gtrsim 13.0$ – 13.5 , which would be consistent with a systematic decrease of column densities over time for overdensities of a given strength. Our data can help to investigate this trend, by uniquely probing the very lowest H I column densities in the Ly α forest at low z . However, given the small sample size and limited number of absorbers with $\log N_{\text{HI}} \gtrsim 13.5$, we cannot obtain a good $\log dN/dN_{\text{HI}}$ slope constraint using just our data, in the framework of the commonly adopted parametric form $dN/dN_{\text{HI}} \propto N_{\text{HI}}^{-\beta}$. Therefore, we employ additional data from the literature to provide a larger comparison sample (larger Δz), with the majority of absorbers at higher N_{HI} to extend the column density range. We used the Ly α forest sample of Lehner et al. (2007a), which contains 270 Ly α systems at $z < 0.44$, covering absorption distance $\Delta z = 2.40$, and a stated completeness to $\log N_{\text{HI}} = 13.2$. They calculated the differential column density distribution for a subsample with $b < 40 \text{ km s}^{-1}$, and errors in b and N_{HI} to < 40 per cent, for a total of 132 absorbers. If we select from our sample in a way that is consistent with these rules, the number of included 3C 273 absorbers at $12.5 \leq \log N_{\text{HI}} < 13.2$ is reduced to a subsample of 11. We calculate a maximum likelihood fit of $\beta = 1.79 \pm 0.07$ for the Lehner et al. subsample over $13.2 \leq \log N_{\text{HI}} \leq 16.5$, with the distribution consistent with a power law to $\sim 2\sigma$ (Kolmogorov–Smirnov probability $P = 0.066$). This is consistent with the Lehner et al. value of $\beta = 1.76 \pm 0.06$. We wish to know whether the weakest absorbers below the completeness limit of Lehner et al. are consistent with a single power law distribution. The 3C 273 sample would comprise only 7.6 per cent of a combined sample with the Lehner et al. data, over only 4.9 per cent of the absorption distance, so it would not contribute much weight to a combined sample. We therefore simply extrapolate our best single power-law fit for the Lehner et al. subsample, and plot two data points from the complete 3C 273 sample covering $12.5 \leq \log N_{\text{HI}} \leq 13.2$ in Fig. 5. The largest deviation shown by the 3C 273 data is in the $12.5 \leq \log N_{\text{HI}} < 12.8$ bin, which is within 0.8σ of the extrapolated fit. The low column density end of the column density distribution is thus consistent with that at $13.2 \leq \log N_{\text{HI}} < 16.5$.

We can probe 0.2-dex lower column density by correcting for the probability of detection at $12.3 \leq \log N_{\text{HI}} < 12.5$ of ~ 50 per cent. Using the same selection criteria as Lehner et al. (2007a), there are three absorbers at $0.020 < z < 0.139$ towards 3C 273 in this extended column density range. We plot both the observed point, which shows signs of a turnover in dN/dN_{HI} , and a factor of 2 correction, which is still consistent to $\sim 1.5\sigma$ at $12.3 \leq \log N_{\text{HI}} < 12.5$ within the extrapolated slope from Lehner et al.

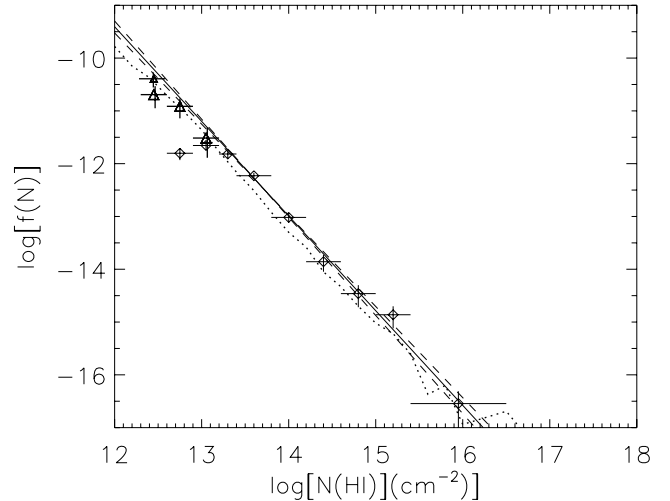


Figure 5. H I column density distribution, $\log[f(N)] = \log d^2N/dXdN_{\text{HI}}$. We plot the $\log N_{\text{HI}} \geq 13.2$, $b < 40 \text{ km s}^{-1}$, ≤ 40 per cent error in b and N_{HI} subsample from Lehner et al. (2007a), recalculating the normalization to correct an error in their fig. 14 (Lehner et al. 2007b). Diamonds: dN/dN_{HI} for Lehner et al. (2007a). Their data are stated complete to $\log N_{\text{HI}} \geq 13.2$, with a turnover at lower N_{HI} . Large triangles: 3C 273 data, with the same Doppler parameter and H I column density restrictions (11 absorbers). The vertical bin centre bars for the $12.3 \leq \log N_{\text{HI}} \leq 12.6$ and $12.8 \leq \log N_{\text{HI}} \leq 13.2$ bins have been slightly offset to the right for clarity. Small triangle: corrected value for $12.3 \leq \log N_{\text{HI}} < 12.6$ bin (six absorbers), assuming a 50 per cent probability of detection, estimated from our simulations. Solid line: our best-fitting slope to the complete Lehner et al. (2007a) data only, $\log[f(N)] = AN_{\text{HI}}^{-\beta}$, $\log A = 12.11^{+0.90}_{-0.91}$, $\beta = 1.793 \pm 0.066$. Dashed lines: 1σ range in slope and normalization. We find the column density distribution at $12.3 \leq \log N_{\text{HI}} < 13.2$ consistent at the ~ 1 – 1.5σ level with an extrapolation from that at $\log N_{\text{HI}} > 13.2$. A normalization error of 0.03 dex is negligible and not included. Dotted line: column density distribution from models of Paschos et al. (2009), table 4, for $z = 0.1$. A normalization correction of $\log f(N) + 0.2$ (60 per cent increase) would best match the data.

Penton et al. (2004) found $\beta = 1.65 \pm 0.07$ (consistent to 1.5σ with our results) over $12.3 \leq \log N_{\text{HI}} \leq 14.5$ at $0.002 < z < 0.069$, based on rest equivalent widths and an assumed Doppler parameter of $b = 25 \text{ km s}^{-1}$. Davé & Tripp (2001) used simulations to correct for incompleteness to show no break in the H I column density distribution to $\log N_{\text{HI}} = 12.6$, and calculated a consistent slope to our value.

4.2 Broad lines

BLAs, with $b > 40 \text{ km s}^{-1}$, have been a subject of interest in the past few years (e.g. Bowen, Pettini & Blades 2002; Penton et al. 2004; Richter et al. 2004; Sembach et al. 2004; Richter et al. 2006a,b; Wakker & Savage 2009, and references therein) because they may be the sign of a significant reservoir of warm-hot IGM (WHIM) gas. Following the convention of Richter et al., we use a sensitivity limit of

$$\frac{N_{\text{HI}}}{b} \gtrsim \frac{3 \times 10^{12}}{(S/N)} \text{ cm}^{-2} (\text{km s}^{-1})^{-1} \approx 7.9 \times 10^{10}, \quad (1)$$

using the S/N per (their) 10 km s^{-1} resolution element in the above expression. This yields $\log N_{\text{HI}}/b \approx 10.9$ given our minimum S/N per pixel of ~ 21 in the Ly α forest, ~ 2 pixel resolution elements and 3.2 km s^{-1} pixel size. Our BLA sample contains three Ly α absorbers in total ($z = 0.07374$, 0.07429 and 0.08763), using the

continuum generated by AUTOVP plus manual modifications around emission lines, and the compound feature detection algorithm. Assigning reliability to BLA detections can involve subjectivity, due to the nature of echelle spectra and variety of detection and continuum fitting techniques. Blending, low S/N ratio, kinematic flows, Hubble broadening and continuum uncertainties could be responsible for up to ~ 50 per cent of BLAs. To keep some subjective standards consistent between different studies, we had one co-author (Kolmogorov–Smirnov), a member of several collaborations which have studied BLAs, examine the BLA candidates. He determined the $z = 0.087632$ absorber to be consistent with some ‘reliable’ samples of recent studies of BLAs e.g. Lehner et al. (2007a). Using this identification to divide the BLA sample into ‘total’ and ‘reliable’, we find $dN/dz = 25 \pm 15$ for the total BLA sample and $dN/dz = 8.5 \pm 8.5$ for the reliable BLA, using a pathlength of $\Delta z = 0.117$ (Fig. 6). These are within 1σ of the values for the total and high quality samples in fig. 2 of Richter et al. (2006a) ($dN/dz \sim 35$ and 15 for total and reliable systems, respectively), which were based on simulated spectra drawn from hydrodynamical simulations.

Given that the 3C 273 sightline is covered by the Sloan Digital Sky Survey (SDSS) spectroscopic galaxy catalogue [data release 6 (DR6); Adelman-McCarthy et al. 2008], we examined the galaxy environment of all BLAs and O VI systems beyond Virgo (Virgo systems being studied in Tripp et al. 2002; Stocke et al. 2006; Wakker & Savage 2009, for example) and not in the 3C 273 host cluster. The one secure BLA and one O VI system each have several listed galaxies with spectroscopic redshifts within 1.5 comoving Mpc impact parameter and $\Delta v \leq 200 \text{ km s}^{-1}$. Their H I redshifts of $z = 0.087632$ and 0.090220 correspond to a line of sight distance of 9.8 local-frame Mpc.

The $z = 0.087632$ BLA has two galaxies with spectroscopic redshifts from the SDSS within 1.3 local-frame Mpc perpendicular to the line of sight (σ_p plane) and $|\Delta v| \leq 75 \text{ km s}^{-1}$ (π axis; Adelman-McCarthy et al. 2008). The next nearest galaxy in the plane of the sky, in increasing velocity space difference, is 2MASX J12271948+0200408 ($\sigma_p = 2.95$ local Mpc, $z = 0.088579$, $|\Delta v| = 261 \text{ km s}^{-1}$). The next closest galaxies within 1.6 local

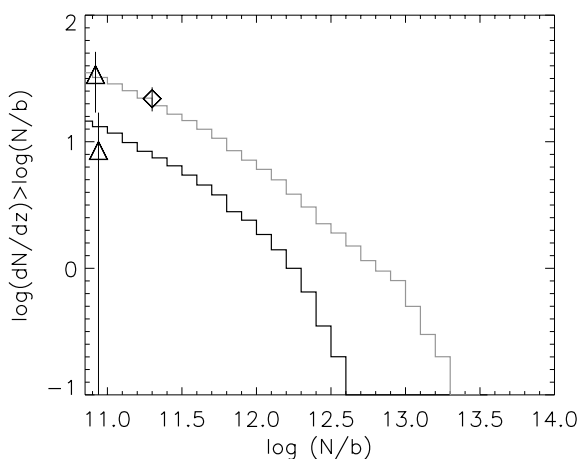


Figure 6. Cumulative number of BLAs per unit redshift, $\log(dN/dz)_{\text{BLA}}$, as a function of the absorption strength, $\log[N(\text{cm}^{-2})/b(\text{km s}^{-1})]$ modelled after Richter et al. (2006a). The total sample is shown in grey and the high-quality sample is plotted in black. The diamond shows the value for $\log(dN/dz)_{\text{BLA}}$ from Richter et al. The triangles show the data from this study, both the total sample (upper) and the secure sample (lower). Vertical error bars have been slightly offset for clarity.

Mpc on the sky are three at $z = 0.0902 \pm 0.0002$, which are close in redshift to the O VI system (see below). We chose 10 000 random points at $0.085 \leq z \leq 0.095$ over $1^\circ \leq \delta \leq 3^\circ$ in declination and $145^\circ \leq \alpha \leq 215^\circ$ in right ascension, which contains 1825 galaxies allowing a 1° border. The SDSS spectroscopic sample covers $15.0 < r < 17.8$ in Petrosian r magnitude, which corresponds to $0.4\text{--}5L^*$ over $0.085 < z < 0.095$ ($M_r^* = -21.4, -21.6$; Blanton et al. 2001; Nakamura et al. 2003). By using the SDSS as its own control sample, systematic undercounting of dense regions due to the maintenance of a minimum fibre distance should affect both the observed and the control samples similarly. We found that a randomly placed absorber would have at least two SDSS galaxies within 1.3 Mpc and $|\Delta v| \leq 75 \text{ km s}^{-1}$ with a probability of $P = 0.006\text{--}0.008$, using the above search regions and varying the redshift limits by ± 0.025 . There is a third galaxy with a redshift in the NASA Extragalactic Data base but not in the SDSS, LDTA 139870, which is 2.2 local-frame Mpc from the line of sight with $\Delta v = 7 \text{ km s}^{-1}$; if it were in the SDSS, the random probability of finding three galaxies within 2.2 Mpc would be the same.

The $z = 0.090220$ O VI absorber ($\log \text{O VI} = 13.18 \pm 0.06$; Tripp et al. 2008) has three SDSS galaxies within 1.6 local-frame Mpc perpendicular to the line of sight and $|\Delta v| \leq 50 \text{ km s}^{-1}$. The next closest galaxies within 2.6 local Mpc on the sky are the three at $z = 0.0876 \pm 0.0002$ discussed with the BLA above, and 2dFGRS N387Z108 ($\sigma_p = 2.84$ local Mpc, $z = 0.0920$, $|\Delta v| = 489 \text{ km s}^{-1}$). We chose 10 000 random points as for the $z = 0.087632$ BLA, and found that a randomly placed absorber would have at least three SDSS galaxies within the same region with a probability of $P = 0.0004\text{--}0.0015$, using the above search regions and varying the redshift limits by ± 0.025 . Properties for galaxies near this O VI absorber and the reliable BLA are listed in Table 5.

The closest three galaxies in velocity space to the $z = 0.087$ BLA (including LEDA 139870, in the NASA Extragalactic Data base but not in the SDSS spectroscopic catalogue) form a rough rhombus with the 3C 273 line of sight, implying that the BLA gas is located in a sheetlike structure at least $\sim 1.1 \times 2$ local Mpc in extent. The multiphase O VI absorber at $z_{\text{H I}} = 0.089898\text{--}0.09110$ is at velocity separation $\Delta v = 682 \text{ km s}^{-1}$ from the $z = 0.087$ BLA. The highest H I column density component of the O VI absorber is $-18 < \Delta v < 61 \text{ km s}^{-1}$ from the three $z \sim 0.09$ galaxies, and they trace an elongated formation ~ 1.5 local-frame Mpc long. The six galaxies are moderately luminous ($L/L^* \approx 0.5 \pm 0.2$). Based on SDSS spectra and colours, and employing spectral energy distribution fitting from PEGASE (Fioc & Rocca-Volmerange 1997), all six galaxies near the BLA and O VI absorber appear to be moderate mass ($9.8 < \log M/M_\odot < 10.9$), old ($\gtrsim 10$ Gyr) and with low star formation rates ($0.1\text{--}1.7 M_\odot \text{ yr}^{-1}$). See Fig. 7 for the relative positions of the 3C 273 sightline and galaxies. We also note that there is a QSO/active galactic nucleus close to that redshift, 2MASX J12260241+0046403, which has $z = 0.083$ ($\Delta v = 1200 \text{ km s}^{-1}$), $b_J = 18.57$ and is 89.3 arcmin or 8.4 local-frame Mpc away (Hao et al. 2005), which may be in a filament with the BLA. The fact that the two absorbers are separated by $\sim 700 \text{ km s}^{-1}$ and that each is on the scale of 1–2 Mpc from moderately bright galaxies may suggest a correlated physical environment for both absorber–galaxy associations.

The BLA and O VI–galaxy distances of 1–2 Mpc are consistent with the correlation lengths for such absorbers with $\sim 0.1\text{--}1.0L^*$ galaxies found from simulations by Ganguly et al. (2008) but are larger than the 100–300 kpc values found by Oppenheimer & Davé (2009). Observationally, the velocity differences between the galaxies and BLA+O VI absorber are well within the $\sim \pm 300\text{--}500 \text{ km s}^{-1}$

Table 5. Galaxies near $z = 0.087$ BLA and 0.090 O VI absorber.

Name	Position (J2000)	z	Δv (km s $^{-1}$) from BLA/O VI ^a	$\Delta\theta'$	D_{\perp} local Mpc	r^b	References ^c
SDSS J122906.84+021348.2	12:29:06.8 +02:13:48	0.087361	-75	10.7	1.05	17.0	2
LEDA 139870	12:28:20.8 +02:21:34	0.087660	7	21.7	2.14	18.0	1,3
SDSS J122828.60+021109.3	12:28:28.6 +02:11:09	0.087717	23	12.4	1.22	17.6	1,3
2MASX J12285184+0206033	12:28:51.9 +02:06:03	0.090046	-18	4.7	0.47	17.1	1,2
2MASX J12280760+0202524	12:28:07.6 +02:02:52	0.090282	47	14.8	1.50	17.3	4
SDSS J122806.93+015959.5	12:28:06.9 +01:59:59	0.090333	61	15.3	1.54	16.7	

^aVelocity difference from O VI system is for highest column density H I component.

^bMagnitude from SDSS DR6 (Adelman-McCarthy et al. 2008). $M_r^* \approx -21.5$ at $z \sim 0.09$ (Blanton et al. 2001; Nakamura et al. 2003) or $r \approx 16.5$.

^cReferences: (1) Morris et al. (1993); (2) Bahcall & Bahcall (1970); (3) Paturel et al. (2000); (4) Tzanavaris, Georgantopoulos & Georgakakis (2006).

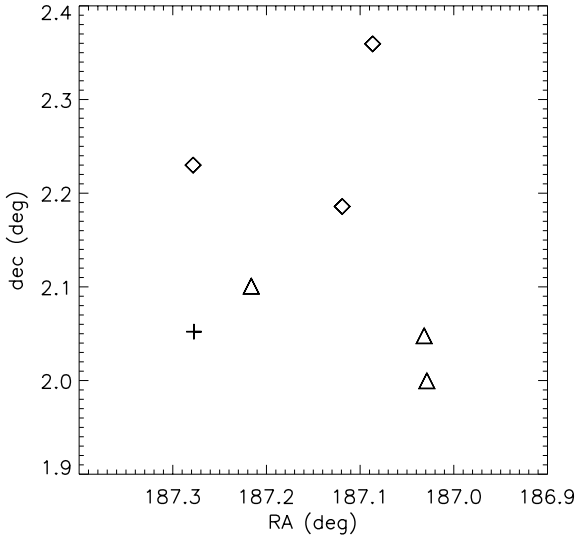


Figure 7. Schematic of 3C 273 (cross) with galaxies within $|\Delta v| \leq 200$ km s $^{-1}$ of the $z = 0.087632$ reliable BLA (diamonds) and $|\Delta v| \leq 50$ km s $^{-1}$ of the $z = 0.090220$ O VI absorber (triangles). At $z = 0.09$ in our adopted cosmology, 0.1 on the sky corresponds to 0.60 local-frame Mpc.

differences used for much of the Wakker & Savage (2009) and Stocke et al. (2006) analyses, almost to the point that any putative absorber–galaxy structures for our two examples appear remarkably coherent over Mpc scales. The galaxy-absorber distances are a factor of several larger than the few $\times 100$ kpc distances found in a large, $z < 0.15$ galaxy-O VI system correlation study by Stocke et al. (2006), and also are large compared to the 350–450 kpc range for O VI absorbers with $L \geq 0.1L^*$ galaxies found by Wakker & Savage (2009) at $z \approx 0$. Wakker & Savage, Prochaska et al. (2006) and Cooksey et al. (2008) found significant variations in the galaxy environment of O VI absorbers. The proximity of the secure BLA and O VI absorber with each other and with luminous galaxies is consistent with the observation of analogous $z \sim 0.06$ – 0.08 O VI–galaxy correlations in large-scale filaments (Tripp et al. 2006) and the WHIM origin of BLA systems (e.g. Richter et al. 2006a,b).

Finally, we compared the general correlation between local galaxy density and integrated $N_{\text{H I}}$ column density for the 3C 273 sightline as in Bowen et al. (2002), and made a Spearman rank correlation and Kendall τ correlation test similar to the one in Paper I. We used 43 galaxies from the NASA Extragalactic Data base within 2° and 2 local-frame Mpc of the 3C 273 sightline at $0.020 < z < 0.139$, where our Ly α detection probability is ≥ 80 per cent. The galaxy sample is inhomogeneous and dominated by SDSS entries, but with no more significant selection effects than

the sample used in Paper I. We do not probe further out in angular distance due to incomplete coverage in the SDSS DR6. We find no evidence of a correlation between galaxies and column density using absorbers with $\log N_{\text{H I}} \geq 12.5$. The Spearman rank coefficient for redshift bin $\Delta z = 0.003$ ($\Delta v \sim 800$ – 900 km s $^{-1}$) is $\rho = 0.283$ with probability $p_\rho = 0.085$, and the corresponding Kendall rank correlation is $\tau = 0.250$ with $p_\tau = 0.027$. Results are insensitive to binning on larger scales, and to lowering the redshift cut-off to $z = 0.11$, because there is only one additional galaxy at $z = 0.138$ below the end of the Ly α forest sensitivity limit. Smaller scale bins are dominated by zero counts of galaxies and H I column densities. This lack of a correlation contrasts with the weak correlation between galaxy number density and summed $N_{\text{H I}}$ column density on 4000–6000 km s $^{-1}$ scales detected towards PKS 0405–123 in Paper I.

The 3C 273 sightline should be probed to $\lesssim 0.1L^*$ up to the QSO redshift to determine whether less luminous galaxies at smaller distances can be associated with the O VI and BLA absorption. Larger cross-correlation samples of BLAs+galaxies and BLAs+O VI systems are needed to quantify further any such trends.

4.3 Clustering and voids

4.3.1 Clustering

Clustering in the low- z Ly α forest has been studied in a number of cases (e.g. Janknecht, Baade & Reimers 2002, and references therein), and weak clustering has been indicated on velocity scales of $\Delta v \lesssim 500$ km s $^{-1}$. We found a clustering signal on the $\Delta v \leq 250$ km s $^{-1}$ scale with STIS E140M data covering $z \lesssim 0.4$ in a sample of 60 Ly α absorbers with $\log N_{\text{H I}} \geq 13.3$ towards PKS 0405–123 (Paper I). The clustering towards 3C 273 is expected to be weaker than for PKS 0405–123 due to the lower $N_{\text{H I}}$ threshold. In a manner similar to Paper I, we established a minimum line separation of $\Delta v = 31$ km s $^{-1}$, based on the observed line separation distribution in the actual data, and made 10 000 random simulations of the 3C 273 line list for comparison to the data, assuming $dN/dz \propto (1+z)^\gamma$, $\gamma = 0.26$ Weymann et al. (1998).

We find clustering at the 3.0σ significance level in the two-point correlation function $\xi(\Delta v)$ for the 21 main sample absorbers with $\log N_{\text{H I}} \geq 12.5$ at $0.020 < z < 0.139$, on the scale of $\Delta v \leq 1000$ km s $^{-1}$. The signal increases in significance to 3.4σ , corresponding to a strength of $\xi(\Delta v < 1000) = 1.0$ for $\log N_{\text{H I}} \geq 12.6$. Poisson counts of the pairs in the bin, which are only an approximation as the pairs between bins are correlated, would indicate 1σ errors of ~ 40 per cent. The simulations give a 99 per cent confidence upper limit of $\xi(\Delta v < 1000) = 1.1$. Based on the 10000 simulated line lists, the probability of the signal

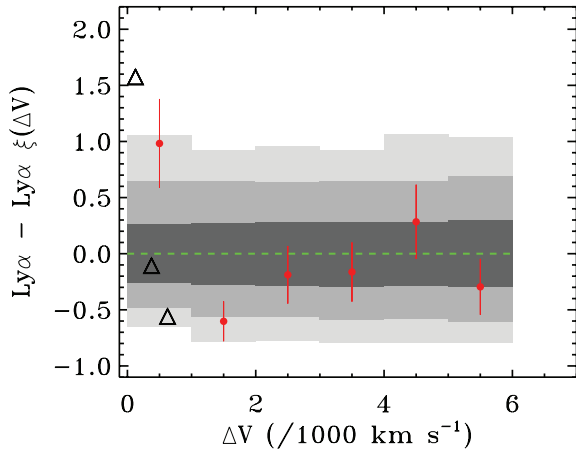


Figure 8. Two-point correlation function for the Ly α sample ($\log N_{\text{H I}} \geq 12.6$) with $\Delta v = 1000 \text{ km s}^{-1}$ binning, which shows the strongest correlation in our sample (3.4σ). Shaded regions denote 68, 95 and 99 per cent confidence limits from 10^4 Monte Carlo simulations. Simulated line lists have been filtered to eliminate pairs with velocity splittings of $\Delta v < 31 \text{ km s}^{-1}$, as in the data. Error bars show example 1σ Poissonian errors. The triangles show expected values from the simulations of Davé et al. (2003) for the same column density threshold; the simulation box size artificially lowers the value of ξ in the higher two velocity bins.

being matched or exceeded is $P = 2.8$ percent. The signal then diminishes in strength at even higher column density thresholds due to the declining sample size. Using the same hydrodynamical simulations for comparison as Paper I (Davé, Katz & Weinberg 2003), we find the measured clustering limits consistent with the predictions (Fig. 8). The τ -step correlation function (Kim et al. 2002) shows no significant signal. The function appears sensitive to rare high column density systems in an otherwise small sample dominated by weak lines, as the only feature of note was contamination at the $\Delta v \sim 70\text{--}90 \text{ km s}^{-1}$ scale for $\tau \geq 0.4$ from the $z = 0.066548$ absorber with $\log N_{\text{H I}} = 14.08$. The restricted Ly α sample with $b < 40 \text{ km s}^{-1}$ and errors in b and $N_{\text{H I}}$ of ≤ 40 per cent only contains 16 systems, and is too small for useful clustering analysis.

Our weak signal in the low z $\log N_{\text{H I}} \gtrsim 12.5\text{--}12.6$ Ly α forest two-point correlation function for $\Delta v < 1000 \text{ km s}^{-1}$ is consistent with the weak clustering predicted by numerical models. However, it is on a larger scale than the signal found towards PKS 0405–123 ($\Delta v < 250 \text{ km s}^{-1}$) for $\log N_{\text{H I}} \geq 13.3$. On a similar $\Delta v = 1000 \text{ km s}^{-1}$ scale, Bowen et al. (2002) found that $N_{\text{H I}}$ column densities summed on 1000 km s^{-1} scales correlate well with the volume density of $M_B \leq -17.5$ galaxies, which was reminiscent of the effect we found in Paper I, albeit on $4000\text{--}6000 \text{ km s}^{-1}$ scales.

There have been no comparable clustering studies in the low-redshift Ly α forest to column density thresholds as low as $\log N_{\text{H I}} = 12.5$. Weak clustering has been found in the low- z Ly α forest for stronger absorbers on scales of up to 500 km s^{-1} . Kirkman et al. (2007) noted non-zero autocorrelations in 74 FOS spectra with 230 km s^{-1} resolution at $z < 1.6$ out to $\Delta v < 500 \text{ km s}^{-1}$ using pixel opacities, which were strongly peaked at $\Delta v < 100 \text{ km s}^{-1}$ for $z < 0.5$ and more broadly peaked at $0.5 < z < 1.5$. Their column density limits arise from sightlines with a variety of sensitivities, but are presumed $\gtrsim 0.5\text{--}1.0$ dex higher in column density than here. Janknecht et al. (2006) noted weak [$\xi(\Delta v) \approx 0.1\text{--}0.4$], marginal signals on scales of $100 < \Delta v < 200 \text{ km s}^{-1}$ and

$1000 < \Delta v < 2000 \text{ km s}^{-1}$ for $12.9 < \log N_{\text{H I}} < 14.0$. Penton et al. (2004) determined a two-point correlation function signal of $\xi(\Delta v < 190 \text{ km s}^{-1}) \sim 3.3$ at the 4.5σ significance level and $\xi(\Delta v < 260 \text{ km s}^{-1}) \sim 2.8$ at 5.6σ significance for rest equivalent width $W_0 \geq 65 \text{ mÅ}$ ($\log N_{\text{H I}} \gtrsim 13.1$ for $b = 25 \text{ km s}^{-1}$). They also found a 3σ excess at $260 < \Delta v < 680 \text{ km s}^{-1}$. However, they found no significant correlation for weak absorbers ($W_0 < 65 \text{ mÅ}$) with either themselves or stronger absorbers, which is consistent with our results. Our 99 per cent confidence limit of $\xi(\Delta v) = 1.1$ at $\Delta v < 1000 \text{ km s}^{-1}$ is at least crudely comparable if not a slightly lower constraint than their four 1σ upper limits of $\xi(\Delta v) \lesssim 2$ over a similar velocity range. A sample size an order of magnitude larger (containing $100\times$ more pairs and roughly reducing bin errors by a factor of 3) would make either more interesting clustering constraints for weak systems or detect a correlation strength predicted in our comparison models. COS data should address this question.

4.3.2 Voids

As in Paper I, we searched for regions in velocity space empty of Ly α systems above a series of H I column density thresholds, and compared them with the frequency of similarly sized gaps in randomized line lists having the same statistical properties as the observations. The most significant gap we find has a line of sight extent of $\Delta v = 8100 \text{ km s}^{-1}$ (120 comoving Mpc) at $0.0901 < z < 0.1200$ for $\log N_{\text{H I}} \geq 12.6$. The probability of such a gap being matched or exceed in a sample with the same number of Ly α lines is $P = 0.006$, using simulated line lists having a Poisson mean of 21. The void persists at more marginal significance for $\log N_{\text{H I}} \geq 12.7$, with $P = 0.022$, and for higher $N_{\text{H I}}$ thresholds the sample becomes too small to be statistically useful. For $\log N_{\text{H I}} \geq 12.5$, the most significant void is over $0.0072 < z < 0.0262$, with $P = 0.023$.

We can use the SDSS DR6 spectroscopic sample (Adelman-McCarthy et al. 2008) as a rough indicator of galaxy overdensity, although by $z \sim 0.12$ it is only probing bright galaxies. We count 0, 3, 9 and 14 galaxies in the SDSS DR6 within 1, 2, 3 and 4 local-frame Mpc, respectively, in the line of sight at $0.0901 < z < 0.1200$. We made counts of galaxies within a grid of 1–4 local-frame Mpc around 10 000 random locations in the same redshift interval, over $140^\circ < \alpha < 225^\circ$ and $-0.25 < \delta < 3.0^\circ$, and found a minimum random probability (for zero galaxies out to a maximum radius of 1.48 Mpc) of $P = 0.88$ for the Ly α forest gap to be in a region up to similarly as dense. The maximum probability is $P = 0.988\text{--}0.989$ for radii $r = 3, 4$ local Mpc. The galaxy environment therefore does not appear significantly underdense, and could in fact be overdense. A comparison with the interval $0.08 < z < 0.09$, which is comparatively rich in that it contains three absorbers and 0, 2, 4 and 6 galaxies within $r < 1, 2, 3$ and 4 local-frame Mpc, respectively, reveals no significant over- or underdensity. (P ranges from 0.771 to 0.922.) Deeper galaxy surveys may reveal more about the relationship between the weakest absorbers and nearby galaxies. We do note from the NASA Extragalactic Data base that a QSO $\sim 1^\circ$ from 3C 273, RX J1230.8+0115 has $V = 14.4$, rest-frame Lyman limit flux $F_{1018\text{Å}} \approx 5 \pm 1 \times 10^{-14} \text{ erg cm}^{-2} \text{ s}^{-1} \text{ Å}^{-1}$ (FUSE program 1099001, PI Sembach), $z = 0.117$ and is 54.3 arcmin or 6.9 local-frame Mpc from the 3C 273 sightline (Read, Miller & Hasinger 1998). For comparison, the QSO SDSS J030435.32–000251.0, which was suggested as causing the $z = 3.05$ He II opacity gap towards Q0302–003 (Heap et al. 2000; Jakobsen et al. 2003), is only 3.0 local-frame Mpc from the line of site and is likely brighter

by several tenths of a dex than RX J1230.8+0115 ($u = 22.35$; a full comparison is beyond the scope of this paper). The $z = 0.1200$ O VI absorber towards 3C 273 is only $\Delta v \sim 800 \text{ km s}^{-1}$ from the RX J1230.8+0115 redshift, and both objects may be located in the same filamentary structure.

Voids in the Ly α forest are rare, and most of the work in the field has been done at high redshift. Few Ly α forest void studies have been done at $z < 1.6$, but they are valuable as comparisons to the galaxy–absorber relation with respect to the inverse question of Ly α absorbers in galaxy voids (e.g. Stocke et al. 2007). In Paper I, we found towards PKS 0405–123 gaps at $0.0320 < z < 0.0814$ of 206 comoving Mpc as defined by $\log N_{\text{H I}} \geq 13.3$ absorbers with probability of random occurrence in shuffled data of $P = 0.0004$, at $0.1030 < z < 0.1310$ for $\log N_{\text{H I}} \geq 13.2$ (113 comoving Mpc, $P = 0.007$) and at $0.0320 < z < 0.0590$ for $\log N_{\text{H I}} \geq 13.1$ (also 113 comoving Mpc, $P = 0.003$). There are several higher redshift voids ($z \sim 1.6$ – 3.2) on the 40–60 Mpc scale for $\log N_{\text{H I}} \sim 13.4$ – 13.5 , which we discussed in Paper I. Given the expected column density versus density perturbation evolution between $z \sim 3$ and ~ 0.2 , the column density levels for which we find our low redshift void(s) towards 3C 273 ($12.5 \leq \log N_{\text{H I}} \leq 12.7$) are comparable to $\log N_{\text{H I}} \approx 14.0$ at $z = 3$ (Section 4.1.1). Our 3C 273 data are thus ~ 0.5 dex too shallow to probe similar density perturbations as used to define the gaps at $z \sim 2$ – 3 . Therefore, we do not consider it unusual to find a slightly larger candidate gap than reported at higher redshift, given the difference in column density sensitivity. We do not find the $0.0901 < z < 0.1200$ region within radius $r \leq 4$ local-frame Mpc of the 3C 273 sightline to be of unusually low galaxy density, based on the SDSS DR6 spectroscopic survey. A more definitive measure of the galaxy environment would require a more sensitive survey.

Although the $0.0901 < z < 0.1200$ gap towards 3C 273 is coincident with RX J1230.8+0115 ($\Delta\theta = 54.3$ arcmin or 6.9 local-frame Mpc), recent analyses of any transverse proximity effect on smaller scales of ~ 1 – 5 Mpc have not indicated significant thinning of the Ly α forest which could produce voids. Possible explanations for the lack of any detections include anisotropic emission (e.g. Hennawi & Prochaska 2007) or the masking of any transverse proximity effect by enhanced density environments around QSOs (Gonçalves, Steidel & Pettini 2008). The correlation length between QSOs and optically thick H I absorbers off the line of sight is $9.2^{+1.5}_{-1.7} h^{-1}$ comoving Mpc at $z \sim 2.5$ (Hennawi & Prochaska), which is three times stronger than the QSO–Lyman break galaxy correlation, would be on the order of the observed distance between RX J1230.8+0115 and the $z = 0.1200$ O VI absorber towards 3C 273. Both objects could therefore mark the same structure. A deep galaxy survey towards the region would confirm this.

Shang, Crofts & Haiman (2007) searched the SDSS for gaps using a pixel opacity technique with limits of transmitted flux $F = 0.6$ – 0.8 at $2.8 < z < 3.9$, which probes rest equivalent widths corresponding to $\log N_{\text{H I}} \approx 13.0$ – 13.5 for $18 < b < 45 \text{ km s}^{-1}$ or overdensities of $\log \rho/\bar{\rho} = -0.2$. They found void sizes of ~ 3 – 35 comoving Mpc, which were in agreement with the standard Λ CDM model for Ly α forest formation. As our Ly α absorber sample does not probe down to the same overdensity level as the Shang et al. search, our results are not inconsistent with theirs. Given the probability of random occurrence of the largest gap we identified, the current paucity of low-redshift data sensitive to $\log N_{\text{H I}} = 12.5$ and the lack of data which probe the same overdensities as Shang et al., future studies with COS should be used to confirm the frequency of large voids.

4.4 The Virgo cluster absorber at $z = 0.00530$

Tripp et al. (2002) established metallicity limits and corresponding physical conditions for the two Virgo cluster absorbers, including the one at $z = 0.00530$. We took the opportunity to re-fit the components. We used nine Lyman series lines through Ly κ (919 Å), and included data from STIS and the revised reductions from the LiF1A, LiF2B, SiC2A and SiC1B *FUSE* channel segments. (The SiC segments covering Ly β were of such low signal that they did not help to give useful constraints.)

We took advantage of the clear Si III feature to set the redshift for the main H I component. Two components provide a satisfactory fit to the data (Fig. 9). The reduced $\chi^2 = 1.19$, though the formal probability of a fit to the data is still < 1 per cent. One component makes a significantly poorer fit, and three are not substantially better (reduced $\chi^2 = 1.234$). A four component fit is marginally worse than the two component fit (reduced $\chi^2 = 1.209$), but suffers from increasing uncertainties in the H I column densities. We therefore adopt a two-component fit with a total H I column density $\log N_{\text{H I}} = 15.70 \pm 0.04$ (1σ error). This is within the 1σ error of the one component fit from the curve of growth measurement of $\log N_{\text{H I}} = 15.77^{+0.12}_{-0.10}$ excluding Ly α , which has the most profound blending effect by the second component, by Sembach et al. (2001). Tripp et al. (2002) adopted $\log N_{\text{H I}} = 15.85^{+0.10}_{-0.08}$, which was the Sembach et al. figure (including Ly α in the curve of growth fit) for their metallicity studies. The conclusions of Tripp et al. about the nature of the $z = 0.0053$ absorber should not be significantly affected. It is possible that the component structure is more complex, but higher signal and resolution far-UV data would be necessary to make a significant improvement, which must wait for a successor to *FUSE*.

5 CONCLUSIONS

We have performed an analysis of the Ly α forest towards 3C 273 based on STIS E140M and a reprocessing and reduction of *FUSE* spectra, and find the following.

(i) We present STIS E140M echelle data for 3C 273, and performed profile fits or measured apparent optical depths for all of the detected Ly α forest over $0 < z < 0.158$, plus intervening metal and Galactic metal absorption systems. We analysed simulated spectra to determine our sensitivity to line detections and resolution of close pairs, and probe to $\log N_{\text{H I}} \approx 12.5$ over most of the spectral range. Our main sample consists of 21 absorbers to $\log N_{\text{H I}} \approx 12.5$ over $0.020 < z < 0.139$.

(ii) The redshift density for the absorbers with column densities $\log N_{\text{H I}} > 14.0$ is consistent with the previous, lower resolution studies, though based only on four absorbers. For absorbers with $13.1 < \log N_{\text{H I}} < 14.0$, the redshift density is $\sim 1.5\sigma$ lower than the mean of comparable low-redshift studies at the same resolution. Absorbers with $\log N_{\text{H I}} \geq 12.5$ and a subset using the same error-limited, $b < 40 \text{ km s}^{-1}$ sample criteria as used by Lehner et al. (2007a) both have a similar redshift density to predictions from numerical models by Paschos et al. (2009) and Davé et al. (1999).

(iii) The Doppler parameter distribution has a mean, median and standard deviation of 28, 27 and 13 km s^{-1} , respectively. There is no significant evidence that line blending affects the distribution. If we choose a restricted sample with errors ≤ 40 per cent in b and $\log N_{\text{H I}}$, and remove absorbers with $b > 40 \text{ km s}^{-1}$, the mean and standard deviation are 24, 24 and 8 km s^{-1} , respectively, which is

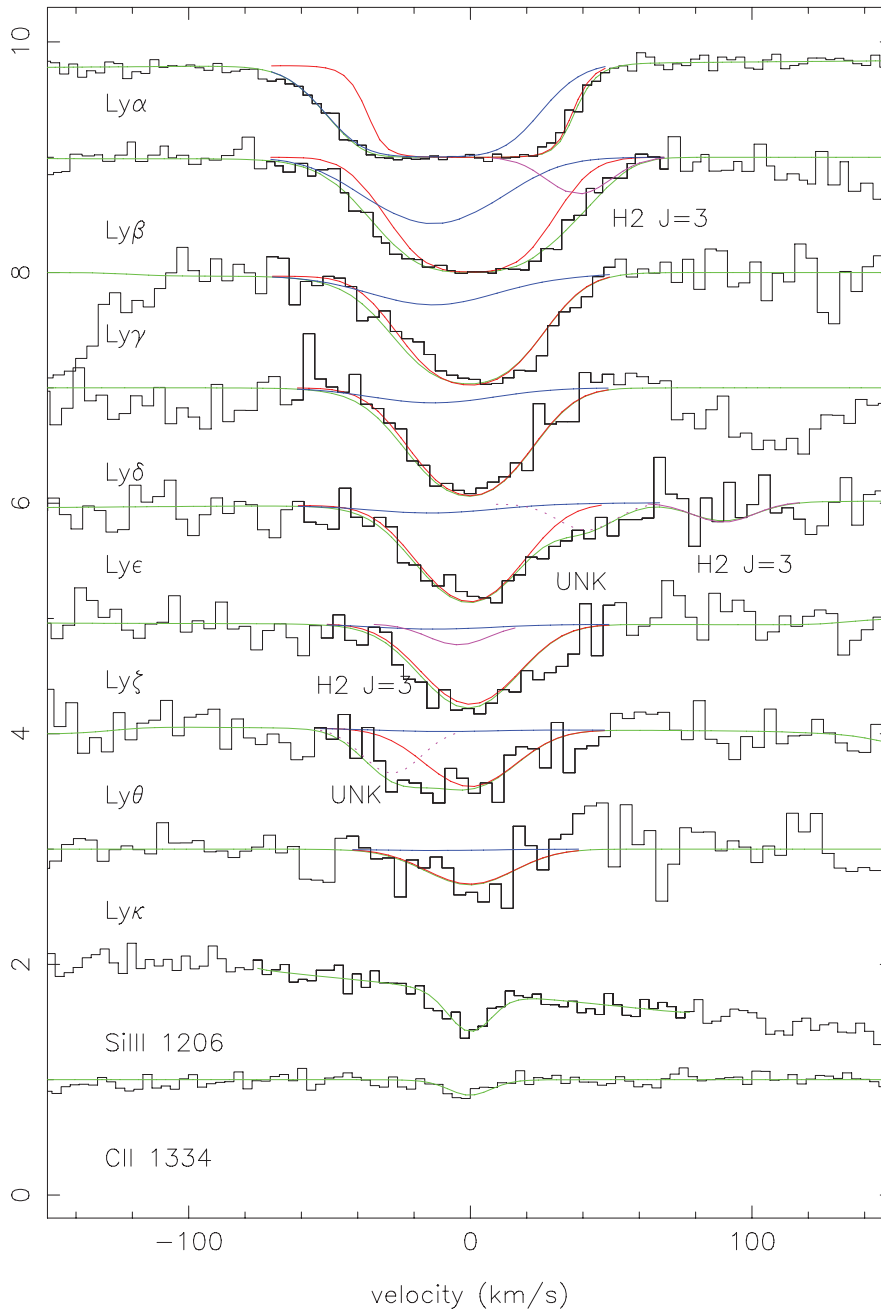
$z = 0.005295$


Figure 9. Two component fit to $z = 0.00530$ Virgo absorber, including Si III 1206 and C II 1334. Green – total profile. Red – higher H I component, at the metal z . Blue – blue component, H I only. Lilac – blends: solid – H₂; dashed – unknown (UNK). Note that the colour sequence from top to underneath is lilac–blue–red–green where there is more than one component (i.e. H I, not metals) so sometimes green especially is obliterated by a component.

consistent with both the main Ly α system sample from Lehner et al. (2007a) and their similarly restricted data set for $b \leq 40 \text{ km s}^{-1}$.

(iv) The H I column density distribution to $\log N_{\text{H I}} = 12.5$ is consistent with a power-law fit to a sample seven times larger covering $13.2 < \log N_{\text{H I}} < 16.5$ from Lehner et al. (2007a). If we correct our sample for the probability of detection at $12.3 < \log N_{\text{H I}} < 12.5$, there is no evidence for a significant break in the power-law fit to $\log N_{\text{H I}} = 12.3$.

(v) We find a total of three BLAs with $b > 40 \text{ km s}^{-1}$ and $\log N_{\text{H I}}/b \approx 10.9$, one of which is deemed reliable. The redshift densities are consistent with results from hydrodynamical simulations by Richter et al. (2006a). The reliable BLA at $z = 0.087632$ is $\approx 700 \text{ km s}^{-1}$ from an O VI absorber in velocity space. The $z = 0.0902$ O VI absorber is in a high galaxy density environment with a probability of being in an equal or richer environment of $P \approx 0.001$, based on galaxy counts in the SDSS DR6. The reliable

BLA is in a marginally overdense environment as well ($P \approx 0.007$), and both may be embedded in the same structure.

(vi) We find evidence for weak clustering in the Ly α forest at 3.4σ significance for $\log N(\text{H I}) \geq 12.6$ from the two-point correlation function on a scale of $\Delta v < 1000 \text{ km s}^{-1}$. The limits obtained are consistent with the clustering expected at that column density limit from hydrodynamical simulations.

(vii) We find evidence for a void in the Ly α forest for $\log N_{\text{H I}} \gtrsim 12.6$ at $0.0901 < z < 0.1200$, with a random probability of occurrence $P = 0.006$. The redshift interval does not cover an unusually low galaxy density environment. The relation between weak absorbers and galaxy environment associated with the 3C 273 and other low- z sightlines should be addressed with deeper galaxy surveys than the SDSS.

(viii) A re-analysis of the $z = 0.0053$ Virgo cluster metal absorption system using both *FUSE* and STIS data reveals velocity structure in the H I absorption which is best fitted by two components. The total H I column density is within 2σ of that used for a previous analysis of the physical properties of the system, whose results are not significantly changed by the adoption of a relatively weak second absorber.

3c 273 provides one of the best probes to very low column density limits at low redshift, and thus a unique probe of halo gas around galaxies in the local Universe. Further studies with COS and a deep, complete galaxy survey will no doubt reveal further details of the galaxy-absorber relation.

ACKNOWLEDGMENTS

This work was partially supported by the STIS IDT through the National Optical Astronomical Observatories and by the Goddard Space Flight Centre. Based on observations obtained with the NASA/ESA *Hubble Space Telescope*, which is operated by the Association of Universities for Research in Astronomy, Inc., under NASA contract NAS 5–26555, and the NASA Far Ultraviolet Spectroscopic Explorer. We also used the NASA Extragalactic Data base (NED). We thank Dave Bowen, Charles Danforth, Rajib Ganguly, Zoltan Haiman, Chris Howk, Jim Lauroesch, Nicolas Lehner, Jon Loveday, Joe Meiring, Emma Ryan-Weber and the late Ervin Williger for useful discussions, manuscript-reading and encouragement, and Eckart Janknecht, Tae-Sun Kim, Jason Prochaska and Philipp Richter for discussions and assistance in assembling comparison data from the literature. We appreciate helpful comments from the referee for improving the presentation of this work. GMW acknowledges support from U. Louisville startup funds, and is grateful for hospitality from Cambridge University, Eötvös University, Konkoly Observatory, Observatoire de Paris-Meudon and Institut d’Astrophysique de Paris during the course of this work.

REFERENCES

- Adelman-McCarthy J. K. et al., 2008, *ApJS*, 175, 297
 Aracil B., Tripp T. M., Bowen D. V., Prochaska J. X., Chen H.-W., Frye B. L., 2006, *MNRAS*, 367, 139
 Bahcall N. A., Bahcall J. N., 1970, *PASP*, 82, 1276
 Bahcall J. N., Jannuzi B. T., Schneider D. P., Hartig G. F., Bohlin R., Junkkarinen V., 1991, *ApJ*, 377, L5
 Bajtlik S., Duncan R. C., Ostriker J. P., 1988, *ApJ*, 327, 570
 Blanton M. L. et al., 2001, *AJ*, 121, 2358
 Bowen D. V., Pettini M., Blades J. C., 2002, *ApJ*, 580, 169
 Cen R., Ostriker J. P., 1999, *ApJ*, 514, 1
 Chen H.-W., Prochaska J. X., Weiner B. J., Mulchaey J. S., Williger G. M., 2005, *ApJ*, 629, L25
 Cooksey K. L., Prochaska J. X., Chen H.-W., Mulchaey J. S., Weiner B. J., 2008, *ApJ*, 676, 262
 Cowie L. L., Songaila A., Kim T.-S., Hu E. M., 1995, *AJ*, 109, 1522
 Croft R. A. C., Weinberg D. H., Katz N., Hernquist L., 1998, *ApJ*, 495, 44
 Danforth C. W., Shull J. M., 2008, *ApJ*, 679, 194
 Davé R., Tripp T. M., 2001, *ApJ*, 553, 528
 Davé R., Dubinski J., Hernquist L., 1997, *New Astron.*, 2, 277
 Davé R., Hernquist L., Katz N., Weinberg D. H., 1999, *ApJ*, 511, 521
 Davé R. et al., 2001, *ApJ*, 552, 473
 Davé R., Katz N., Weinberg D. H., 2003, in Rosenberg J. L., Putman M. E., eds., *The IGM/Galaxy Connection: The Distribution of Baryons at $z = 0$* . Kluwer, Dordrecht, p. 271
 Dixon W. V. et al., 2007, *PASP*, 119, 527
 Dressel L. et al., 2007, *STIS Data Handbook, Version 5.0*. STScI, Baltimore
 Fioc M., Rocca-Volmerange B., 1997, *A&A*, 326, 950
 Ganguly R., Cen R., Fang T., Sembach K., 2008, *ApJ*, 678, L89
 Gonçalves R. S., Steidel C. C., Pettini M., 2008, *ApJ*, 676, 816
 Grogin M. A., Geller M. J., Huchra J. P., 1998, *ApJS*, 119, 277
 Hao L. et al., 2005, *AJ*, 129, 1783
 Heap S. R., Williger G. M., Smette A., Hubeny I., Sahu M. S., Jenkins E. B., Tripp T. M., Winkler J. N., 2000, *ApJ*, 534, 69
 Heap S. R., Williger G. M., Davé R., Weymann R. J., Jenkins E. B., Tripp T. M., 2002, in Mulchaey J., Stocke J., eds., *Proc. ASP Conf. 254, Extragalactic Gas at Low Redshift*. Astron. Soc. Pac., San Francisco, p. 63
 Heap S. R., Williger G. M., Davé R., Weymann R. J., 2003, in Rosenberg J. L., Putman M. E., eds., *ASSL Conf. Proc. 281, The IGM/Galaxy Connection: The Distribution of Baryons at $z = 0$* . Kluwer, Dordrecht, p. 75
 Hennawi J. F., Prochaska J. X., 2007, *ApJ*, 655, 735
 Hoffman G. L., Lu N. Y., Salpeter E. E., Connell B. M., Fromhold-Treu R., 1998, *ApJ*, 500, 789
 Impy C. D., Petry C. E., Flint K. P., 1999, *ApJ*, 524, 536
 Jakobsen P., Jansen R. A., Wagner S., Reimers D., 2003, *A&A*, 397, 891
 Janknecht E., Baade R., Reimers D., 2002, *A&A*, 391, L11
 Janknecht E., Reimers D., Lopez S., Tytler D., 2006, *A&A*, 458, 427
 Kim T.-S., Carswell R. F., Cristiani S., D’Odorico S., Giallongo E., 2002, *MNRAS*, 335, 555
 Kirkman D., Tytler D., 1997, *AJ*, 484, 672
 Kirkman D., Tytler D., Lubin D., Charlton J., 2007, *MNRAS*, 376, 1227
 Lanzetta K., Bowen D. V., Tytler D., Webb J. K., 1995, *ApJ*, 442, 538
 Lehner N., Savage B. D., Richter P., Sembach K. R., Tripp T. M., Wakker B. P., 2007a, *ApJ*, 658, 680
 Lehner N., Savage B. D., Richter P., Sembach K. R., Tripp T. M., Wakker B. P., 2007b, *ApJ*, 674, 613
 Lu L., Sargent W. L. W., Womble D. S., Takada Hidai M., 1996, *ApJ*, 472, 509
 Misawa T., Tytler D., Iye M., Kirkman D., Suzuki N., Lubin D., Kashikawa N., 2007, *AJ*, 134, 1634
 Morris S. L., Weymann R. J., Savage B. D., Gilliland R. L., 1991, *ApJ*, 377, L21
 Morris S. L., Weymann R. J., Dressler A., McCarthy P. J., Giovanelli R., Irwin M., 1993, *ApJ*, 419, 524
 Morton D. C., 2003, *ApJS*, 149, 205
 Murdoch H. S., Hunstead R. W., Pettini M., Blades J. C., 1986, *ApJ*, 309, 19
 Nakamura O., Fukugita M., Yasuda N., Loveday J., Brinkmann J., Schneider D. P., Shimasaku K., SubbaRao M., 2003, *AJ*, 125, 1682
 Narayanan A., Wakker B. P., Savage B. D., 2009, *ApJ*, 703, 74
 Oppenheimer B. D., Davé R., 2009, *MNRAS*, 395, 1875
 Paschos P., Jena T., Tytler D., Kirkman D., Norman M. L., 2009, *MNRAS*, 399, 1934
 Paturel G., Fang Y., Petit C., Garnier R., Rousseau J., 2000, *A&AS*, 146, 19
 Penton S. V., Shull J. M., Stocke J. T., 2004, *ApJS*, 152, 29
 Pettini M., Ellison S. L., Schaye J., Songaila A., Steidel C. C., Ferrara A., 2001, *A&AS*, 277, 555

- Prochaska J. X., Weiner B. J., Chen H.-W., Mulchaey J., 2006, *ApJ*, 643, 680
- Rauch M., Carswell R. F., Webb J. K., Weymann R. J., 1993, *MNRAS*, 260, 589
- Read M. A., Miller L., Hasinger G., 1998, *A&A*, 335, 121
- Richter P., Savage B. D., Tripp T. M., Sembach K. R., 2004, *ApJS*, 153, 165
- Richter P., Fang T., Bryan G. L., 2006a, *A&A*, 451, 767
- Richter P., Savage B. D., Sembach K. R., Tripp T. M., 2006b, *A&A*, 445, 827
- Rosenberg J. L., Ganguly R., Giroux M. L., Stocke J. T., 2003, *ApJ*, 591, 677
- Ryan-Weber E., 2006, *MNRAS*, 367, 1251
- Salpeter E. E., Hoffman G. L., 1995, *ApJ*, 441, 51
- Salzer J. J., 1992, *AJ*, 103, 385
- Savage B. D., Sembach K. R., 1991, *ApJ*, 379, 245
- Savage B. D., Lehner N., Wakker B. P., Sembach K. R., Tripp T. M., 2005, *ApJ*, 626, 776
- Savaglio S. et al., 1999, *ApJ*, 515, L5
- Schaye J., 2001, *ApJ*, 559, 507
- Sembach K. R., Savage B. D., 1992, *ApJS*, 83, 147
- Sembach K. R., Howk J. C., Savage B. D., Shull J. M., Oegerle W. R., 2001, *ApJ*, 561, 573
- Sembach K. R., Tripp T. M., Savage B. D., Richter P., 2004, *ApJS*, 155, 351
- Shang C., Crotts A., Haiman Z., 2007, *ApJ*, 136, 145
- Shull M., Stocke J. T., Penton S., 1996, *AJ*, 111, 72
- Shull J. M. et al., 2000, *ApJ*, 538, L13
- Songaila A., Cowie L. L., 1996, *AJ*, 112, 335
- Stocke J., Shull J. M., Penton S., Donahue M., Carilli C., 1995, *ApJ*, 451, 24
- Stocke J. T., Keeney B. A., McLin K. M., Rosenberg J. L., Weymann R. J., Giroux M. L., 2004, *ApJ*, 609, 94
- Stocke J. T., Penton S. V., Danforth C. W., Shull J. M., Tumlinson J., McLin K. M., 2006, *ApJ*, 641, 217
- Stocke J. T., Danforth C. W., Shull J. M., Penton S. V., Giroux M. L., 2007, *ApJ*, 671, 146
- Thom C., Chen H.-W., 2008, *ApJS*, 179, 37
- Tripp T., Lu L., Savage B. D., 1998, *ApJ*, 508, 200
- Tripp T. M., Giroux M. L., Stocke J. T., Tumlinson J., Oegerle W. R., 2001, *ApJ*, 563, 724
- Tripp T. M. et al., 2002, *ApJ*, 575, 697
- Tripp T. M., Aracil B., Bowen D. V., Jenkins E. B., 2006, *ApJ*, 643, L77
- Tripp T. M., Sembach K. R., Bowen D. V., Savage B. D., Jenkins E. B., Lehner N., Richter P., 2008, *ApJS*, 177, 39
- Tytler D., 1987, *ApJ*, 321, 49
- Tzanavaris P., Georgantopoulos I., Georgakakis A., 2006, *A&A*, 454, 447
- Ulrich M. H. et al., 1980, *MNRAS*, 192, 561
- Wakker B. P., Savage B. D., 2009, *ApJS*, 182, 378
- Webb J. K., 1987, PhD thesis, Cambridge Univ. Press, Cambridge
- Weymann R. J., Rauch M., Williams R., Morris S., Heap S., 1995, *ApJ*, 438, 650
- Weymann R. J. et al., 1998, *ApJ*, 506, 1
- Williger G. M., Heap S. R., Weymann R. J., Davé R., Ellingson E., Carswell R. F., Tripp T. M., Jenkins E. B., 2006, *ApJ*, 636, 631 (Paper I)

APPENDIX A: A COMPARISON WITH THE LINE LIST FROM DANFORTH & SHULL (2008)

Danforth & Shull (2008) published a study of a large sample of QSO absorbers, including the line list for a data set analysed in detail in this work. There are a number of differences in the reduction and analysis. Danforth & Shull used CALFUSE 2.4 to reduce the *FUSE* data, whereas we used CALFUSE 3.1.3 (Dixon et al. 2007), which has many changes, including a significant improvement in the wavelength calibration from version 2.4. Danforth & Shull normalized the data in 10-Å segments centred on IGM absorbers and binned the

FUSE and smoothed the STIS data by 3 pixels each, whereas we used a mainly automated continuum-fitter with manual adjustments around emission lines and did not bin or smooth. Danforth & Shull used a combination of apparent optical depth (Sembach & Savage 1992), curve of growth concordance plots and Voigt profile fitting, whereas we mainly used Voigt profile fits and only used apparent optical depth to establish lower limits for saturated metal transitions. Danforth & Shull tended to treat blends which they could not separate unambiguously as single absorbers, whereas our normal procedure is to add components when the existing Voigt profile fit has a probability of matching the data of $P < 0.01$.

We matched absorbers from the Danforth & Shull list with ours, and combined apparently blended absorbers in our line list in velocity space (up to $\Delta v \sim 70 \text{ km s}^{-1}$) by summing their H I column densities. We display the comparison for 20 systems in common in Fig. A1. For the plot we use the errors in $\log N_{\text{HI}}$ for our fits, and also the Doppler value and corresponding errors, for the highest N_{HI} component. The H I column densities show a good match within 1σ errors. The Doppler parameters show more scatter, which likely arises from the finer structure decomposition in this study, but are still largely consistent within 1σ errors.

Absorbers in one list but not the other or potentially suspect absorbers are as follows.

$z = 0.002630$. This is a broad line which Danforth & Shull do not list. We need this component for a proper fit to the Galactic Ly α profile, which we fitted simultaneously with the IGM components in the wing. It is below the minimum redshift for any of our statistical analyses.

$z = 0.007588$. This feature is included by Danforth & Shull as well. It is in the wing of Galactic H I, and shows a double minimum. The complex has $\sim 3\sigma$ significance overall. We include it due to its contribution to a fit to the Galactic H I complex, but note that the profile is atypical and may indicate a blend of two weaker features.

$z = 0.054399$. This is a weak line which Danforth & Shull do not list. It is below our 80 per cent probability of detection threshold of $\log N_{\text{HI}} = 12.5$, but is used for the H I column density extrapolation to $\log N_{\text{HI}} = 12.3$.

$z = 0.06051$. This is a weak line from Danforth & Shull which we do not list due to its low significance. It contains a small noise spike halfway through the feature, and has a square profile and flat minimum.

$z = 0.064078$. This is a shallow, moderately broad feature which Danforth & Shull do not list. We find satisfactory constraints on the column density and Doppler parameter such that we use it in our statistical samples.

$z = 0.073738$ and 0.074286 . These are broad, shallow feature which Danforth & Shull do not list. Their high Doppler parameters of $b = 64 \pm 15$ and $51 \pm 14 \text{ km s}^{-1}$ make us omit them from our restricted sample analysis, to be consistent with the Lehner et al. (2007a) $b < 40 \text{ km s}^{-1}$ sample criteria. The $z = 0.073738$ system is unlikely to be Galactic O I*, since its redshifted corrected position is just outside the O I1032 profile. There may be a better case for O I** being the $z = 0.07429$ feature, since it falls in the ground state profile, and there is possibly O I* in the red wing of Si II 1304. However, neither agree particularly well in position with C II*, so unless they would be at significantly different velocities (which is not suggested by the relative positions of the C II/O I centroids) then we doubt that the O I*, O I** identifications apply.

$z = 0.085882$. This is a broad, shallow feature which Danforth & Shull do not list. It is below our 80 per cent probability of detection threshold of $\log N_{\text{HI}} = 12.5$, but is used for the H I column density extrapolation to $\log N_{\text{HI}} = 12.3$.

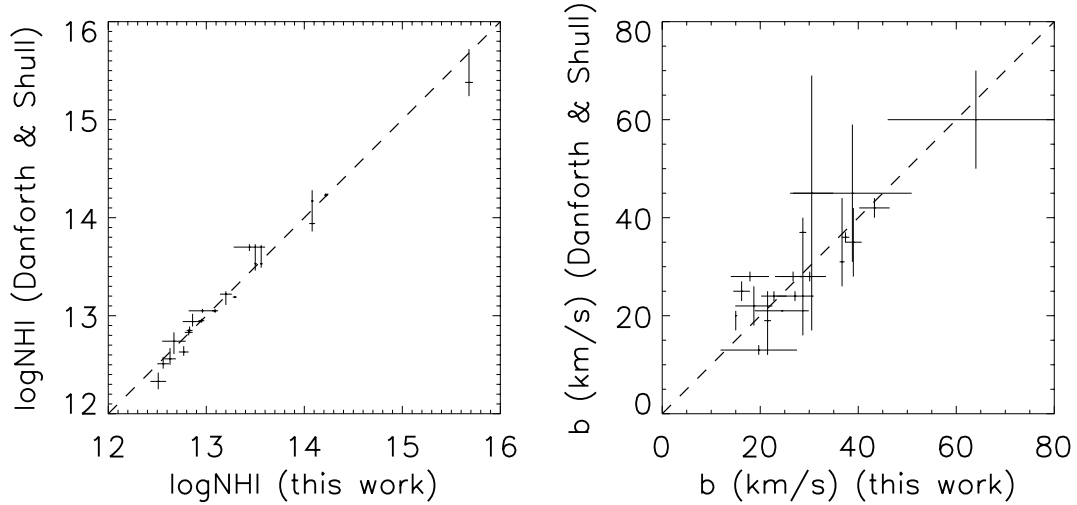


Figure A1. Comparison of H I column density and Doppler parameter for 20 absorbers in common between Danforth & Shull (2008) and this work, with 1σ error bars. Column densities have been summed in the case of fitted complexes in this work spanning $\Delta v \lesssim 70 \text{ km s}^{-1}$. However, column density errors for this study have been retained for the highest N_{HI} component, as are the Doppler parameters and errors. Fits are generally consistent within 1σ errors. Differences are qualitatively understandable in that Danforth & Shull have slightly higher column densities and Doppler parameters due to their not using as fine component structure as in this paper.

$z = 0.109141$. This is a shallow, round-bottomed feature which Danforth & Shull do not list. We use it in our extrapolation of the H I column density distribution to $\log N_{\text{HI}} = 12.3$, but in no other statistical sample.

$z = 0.13943$. Danforth et al. list it, but we find it less plausible. It is assymetrical and contains a noise spike. The significance is $\sim 3\sigma$, and depends strongly on the integration bounds.

$z = 0.141676$ and 0.150204 . These are broad, shallow features which Danforth & Shull do not list. They have $\sim 3\sigma$ and 4.5σ significance, respectively. They fall on Ly α emission and within our definition of the proximity effect zone ($\Delta v < 5000 \text{ km s}^{-1}$),

and are also below our 80 per cent probability detection limit. We do not use them for any analysis.

$z = 0.157787$. This is a distinct absorber with a hint of an extended red wing, noted in Tripp et al. (2008) in association with O VI. We fitted the feature with one component. Danforth & Shull do not list it, presumably because it falls within their definition of the proximity effect zone ($\Delta v < 1500 \text{ km s}^{-1}$).

This paper has been typeset from a $\text{\TeX}/\text{\LaTeX}$ file prepared by the author.